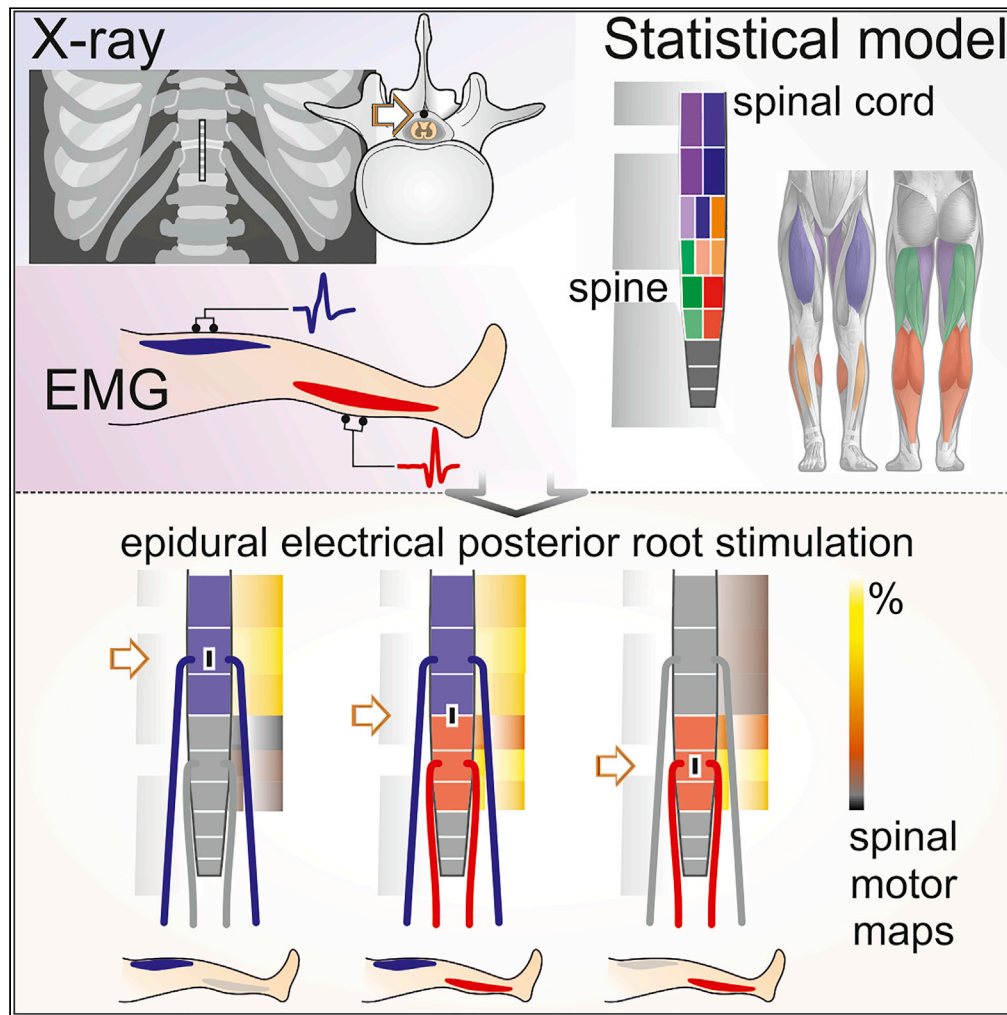


Article

Spinal motor mapping by epidural stimulation of lumbosacral posterior roots in humans



Ursula S. Hofstoetter, Ivan Perret, Aymeric Bayart, Peter Lackner, Heinrich Binder, Brigitta Freundl, Karen Minassian

ursula.hofstoetter@meduniwien.ac.at

Highlights

Spinal motor maps are created by epidural lumbosacral posterior root stimulation

Muscle-specific stimulation sites coincide with segmental motoneuron pool locations

Lower-extremity motor recruitment is alike in different upper motoneuron disorders

Intraoperative mapping predicts postoperative selectivity of epidural stimulation

Hofstoetter et al., iScience 24, 101930
January 22, 2021 © 2020 The Author(s).
<https://doi.org/10.1016/j.isci.2020.101930>



Article

Spinal motor mapping by epidural stimulation of lumbosacral posterior roots in humans

Ursula S. Hofstoetter,^{1,3,*} Ivan Perret,¹ Aymeric Bayart,¹ Peter Lackner,² Heinrich Binder,² Brigitta Freundl,² and Karen Minassian¹

Summary

Epidural electrical stimulation of the spinal cord is an emergent strategy for the neurological recovery of lower-extremity motor function. Motoneuron pools are thought to be recruited by stimulation of posterior roots. Here, we linked electromyographic data of epidurally evoked lower-extremity responses of 34 individuals with upper motoneuron disorders to a population model of the spinal cord constructed using anatomical parameters of thousands of individuals. We identified a relationship between segmental stimulation sites and activated spinal cord segments, which made spinal motor mapping from epidural space possible despite the complex anatomical interface imposed by the posterior roots. Our statistical approach provided evidence for low-threshold sites of posterior roots and effects of monopolar and bipolar stimulation previously predicted by computer modeling and allowed us to test the impact of different upper motoneuron disorders on the evoked responses. Finally, we revealed a statistical association between intraoperative and postoperative mapping of the spinal cord.

Introduction

Epidural electrical stimulation (EES) of the spinal cord is broadly known as a treatment for chronic intractable pain of the trunk and limbs (Krames et al., 2009; Rock et al., 2019; Shealy et al., 1967). For this indication, EES is generally applied at C2–C3 vertebral levels for neck and upper-extremity pain (Rock et al., 2019; Schoen et al., 2017) and at T8–T10 for lower-back and lower-extremity coverage (Air et al., 2012; Shils and Arle, 2018) and is associated with the stimulation of ascending fiber branches of cutaneous afferents in the spinal cord dorsal columns (Holsheimer, 1998; Shils and Arle, 2012; Tulgar et al., 1993). Its use in motor disorders has a history nearly as long as in pain (Cook and Weinstein, 1973; Illis et al., 1976; Minassian et al., 2012), with neuromodulation of spasticity having been the initial interest in spinal cord injury (SCI) (Barolat et al., 1995; Dimitrijevic et al., 1986; Pinter et al., 2000; Richardson et al., 1979). Recent studies of EES demonstrated unprecedented improvements of lower-extremity motor function thought to be irreversibly lost due to chronic SCI and signaled a new era of application in motor disorders (Calvert et al., 2019b). Following the observation that EES can enable volitionally initiated activation of otherwise paralyzed muscles (Angeli et al., 2014; Harkema et al., 2011), the facilitation of overground walking was the next breakthrough finding (Angeli et al., 2018; Gill et al., 2018; Wagner et al., 2018). These first advances in demonstrating efficacy have partially preceded the understanding of the underlying principles. The vast neuroprosthetics, neuroanatomical, and physiological knowledge gained from the application in pain (Barolat et al., 1993; Gildenberg, 2009; He et al., 1994; Shils and Arle, 2018) cannot be translated to the use for motor function. All contemporary studies had placed the epidural electrodes at T11–L1 vertebral levels guided by monitoring of evoked responses, based on the assumption that specific spinal cord segments innervating lower-extremity muscles could be targeted with electrodes directly overlying them (Calvert et al., 2019a; Harkema et al., 2011; Murg et al., 2000; Wagner et al., 2018). However, no study so far was designed to demonstrate whether such functional monitoring would identify the anatomical stimulation site relative to the activated lumbosacral spinal cord segments. Motor effects of EES are associated with the stimulation of proprioceptive fibers within posterior roots (Capogrosso et al., 2013; Dimitrijevic et al., 1980; Formento et al., 2018; Minassian et al., 2016; Wagner et al., 2018). There is a dissociation between the segmental anatomy of the lumbosacral spinal cord and the longitudinally running posterior roots, which have a complex topographic anatomy (Wall et al., 1990) and can be stimulated from a wide

¹Center for Medical Physics and Biomedical Engineering, Medical University of Vienna, 1090 Vienna, Austria

²Neurological Center, Klinik Penzing Wiener Gesundheitsverbund, 1140 Vienna, Austria

³Lead contact

*Correspondence: ursula.hofstoetter@meduniwien.ac.at

<https://doi.org/10.1016/j.isci.2020.101930>



range of rostrocaudal electrode positions (Ladenbauer et al., 2010; Rattay et al., 2000) due to their intrathecal lengths of up to 16 cm (Lang and Geisel, 1983) and the current spread within the cerebrospinal fluid (Capogrosso et al., 2013). In addition, imaging techniques cannot identify segmental electrode positions.

Here, we sought to map the human lumbosacral spinal cord by implementing a relationship between the statistically estimated anatomical, segmental site of a stimulating epidural cathode and the segments of activated motoneuron pools. To achieve this goal, we linked vertebral cathode sites and evoked responses of multiple lower-limb muscles involved in locomotion to an anatomical model of the vertebral locations of the lumbosacral spinal cord and segmental innervation probabilities, constructed using parameters of thousands of subjects from literature. Electromyographic (EMG) responses evoked by low-frequency EES applied from vertebral locations ranging from T9 to L1 were analyzed. Data were derived from 34 individuals with upper motoneuron disorders, a sample size that, for the first time, made sound statistical analysis possible. We hypothesized that—despite the anatomically complex interface imposed by the posterior roots—threshold stimulation would precisely map the rostrocaudal locations of the anatomically separate motoneuron pools innervating the rectus femoris (L2–L4) and the triceps surae muscle group (L5–S2), based on theoretically predicted low-threshold sites of proprioceptive root fibers at their segmental entries (Capogrosso et al., 2013; Ladenbauer et al., 2010; Rattay et al., 2000; Struijk et al., 1993). We extended our analysis to multiple lower-extremity muscles with overlapping segmental innervations and tested whether EMG amplitudes of evoked responses would reflect the segmental spinal cord organization. Our further goals were to inquire the impact of the type and severity of upper motoneuron disorder as well as of mono- and bipolar EES on the recruitment of the evoked responses. Finally, we statistically evaluated the association between intra- and postoperative mapping of the spinal cord.

Results

Spinal cord model and segmental positions of stimulating cathodes

We interfaced EMG data of epidurally evoked lower-extremity responses of 34 subjects with upper motoneuron disorders (Table S1) with the segmental organization of the lumbosacral spinal cord pursuing a statistical approach. We constructed a straight-line geometrical model of the spine from the lower endplate of the L1- to the upper endplate of the T10-vertebral body from anatomical dimensions (Figure 1A; Tables S2 and S3). Vertebral body and intervertebral disc heights increased monotonically from T10 to L1. The total height of the model was 108.7 mm. We incorporated a straight-line model of the lumbosacral spinal cord (Figure 1B; Tables S4 and S5). The segmental heights decreased monotonically in caudal direction. The total heights of the lumbar and sacral spinal cord amounted to 49.8 mm and 26.5 mm, respectively. The termination of the conus medullaris was defined at the lower third of the L1-vertebral body (median value derived from a population of $n = 4,797$ samples from literature, IQR from the L1/L2-intervertebral disc to the upper third of the L1-vertebral body; Table S6). We estimated that the mean termination level of our 34 subjects would be within ± 5.7 mm of the model's value, i.e., of the population, with a confidence of 95% (see Transparent Methods). We added segmental innervation probabilities of the lower-extremity muscles of interest (Figure 1C). Motoneuron pools of the medial and anterior thigh muscles (adductors, Add; rectus femoris, RF; L2–L4 spinal cord segments) were segmentally separate from the posterior lower-leg muscles (triceps surae muscle group, TS; L5–S2). The tibialis anterior (TA) motoneuron pool overlapped partially with the segmental locations of the other motoneuron pools. The segmental innervation of the hamstrings muscle group (Ham) was broader than that of the other muscles studied. We identified the vertebral positions of all tested cathodes of the midline-placed epidural linear leads from X-rays and transformed them into longitudinal coordinates in the straight-line spine model (Figure S1). This was a necessary step to link evoked responses to the segmental stimulation site, which cannot be deduced from imaging techniques. The distribution of tested cathode sites ($n = 134$, 34 subjects) ranged from the T9/T10-intervertebral disc to the lower endplate of the L1-vertebral body, covering the low-thoracic as well as all lumbar and sacral spinal cord segments (Figure 1D).

The epidurally evoked responses are posterior root-muscle reflexes

We had previously demonstrated the reflex nature of responses evoked with midline-placed cylindrical electrodes as used here (Hofstoetter et al., 2018; Minassian et al., 2004, 2016). Post-stimulation depression of responses to double stimuli and unchanged onset latencies with increasing stimulation amplitude affirmed that, across stimulation sites and amplitudes, this was also the case for the present dataset (see Data S1 and Figure S2). EES would hence map the segmental anatomy of the lumbosacral spinal cord through the electrical stimulation of proprioceptive afferents.

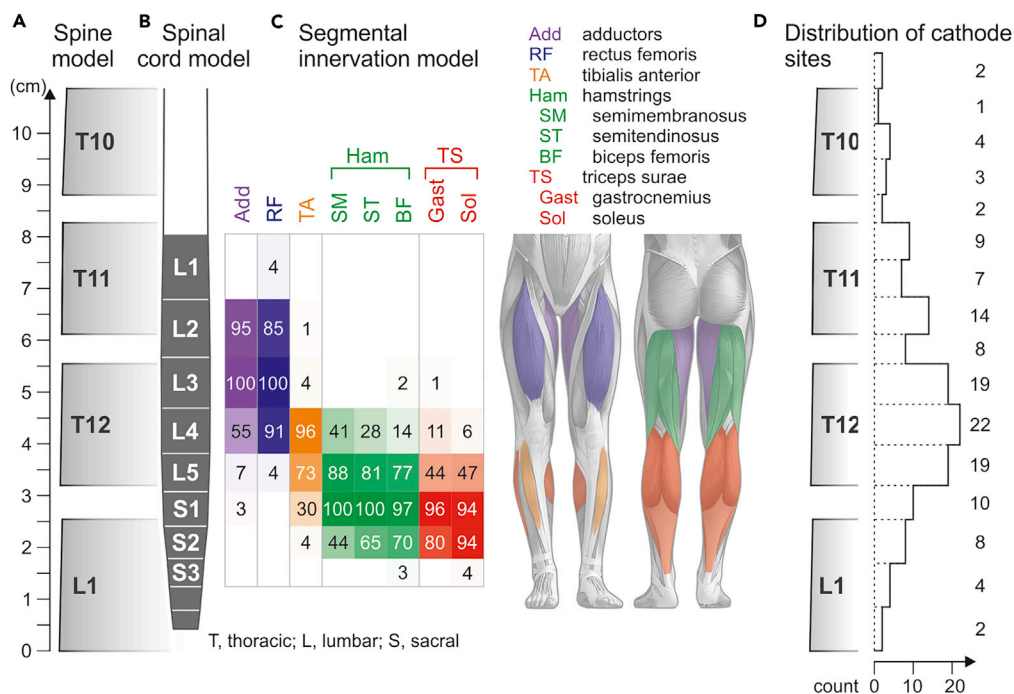


Figure 1. Spinal cord and segmental innervation model

(A) Straight-line anatomical model of the spine, defined by vertebral body and intervertebral disc heights.

(B) Straight-line model of the lumbosacral spinal cord aligned with the spine model.

(C) Segmental innervation probabilities (0%–100%) of Add, RF, TA, SM, ST, BF, Gast, and Sol, reflected by the opacity of the respective colors. Sources and values considered in the spine model are specified in Tables S2 and S3, those of the spinal cord model in Tables S4–S6.

(D) Distribution of vertebral cathode positions tested; numbers are counts per bin (intervertebral disc or upper, middle, or lower third of vertebral body). Cathode positions tested in different monopolar or bipolar setups in a given subject were counted only once.

PRM reflexes evoked from a wide range of epidural cathode sites

EMG responses of RF and TS evoked by EES with threshold amplitude are illustrated in Figure 2A. The responses reflected the segmental anatomy of the lumbosacral spinal cord despite their elicitation through an anatomically complex interface (Figure 2B). Although responses could be evoked by stimulation applied from a wide rostrocaudal range, the largest EMG potentials were elicited when the estimated segmental cathode sites were located over the segmental locations of the respective motoneuron pools in the anatomical model.

Mapping of the lumbosacral spinal cord based on PRM-reflex thresholds

We classified the vertebral cathode positions of 570 EMG datasets (34 subjects, two legs, multiple electrode setups; monopolar stimulation, $n = 72$; bipolar stimulation, $n = 498$) into four categories based on the elicitation of RF- and TS-posterior root-muscle (PRM) reflexes and their relative thresholds (no responses, RF bias, non-selective, TS bias; see Figure 3 and Transparent Methods). RF and TS were chosen as the key muscles in this analysis because of their largely separate segmental innervations. We found a significant difference between the rostrocaudal cathode distributions (registered coordinates in the model) of the four categories (Kruskal-Wallis test, $\chi^2(3) = 97.688$, $p < .001$, $r = .414$; Figure 3A). Post-hoc comparisons revealed differences between each of the categories (non-selective vs. TS bias, $p = .016$; all other $p < .001$). The no-responses category was associated with the most rostral cathode positions, with the median at the L1 spinal cord segment. The RF-bias category had a median cathode site at the L3 segment with an IQR covering the L2–L4 segments. In 28.0% of the datasets within this category, TS responses were not evoked even with maximum stimulation amplitude. Non-selective recruitment of RF and TS resulted from a cathode site distribution with its median at the L4 segment. The TS-bias category was associated with the most caudal cathode sites, with the median at the L5 segment and an IQR covering

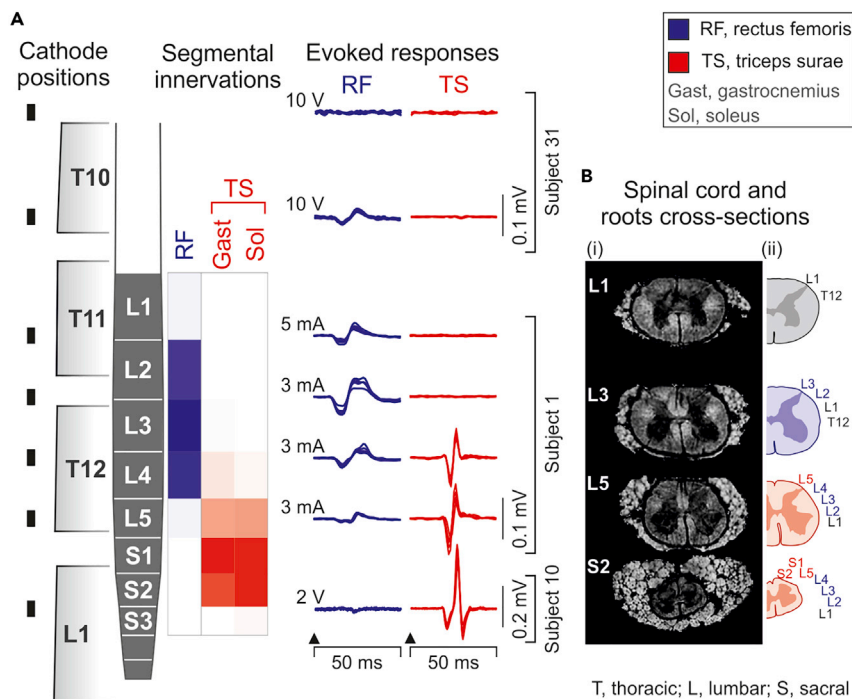


Figure 2. Mapping the segmental lumbosacral spinal cord anatomy by epidurally evoked muscle responses—exemplary results

(A) EMG responses of RF and TS evoked by epidural stimulation with threshold amplitude, aligned with the respective rostrocaudal cathode positions (black rectangles) and segmental innervations. Neither muscle was recruited from the most rostral site with maximum stimulation (10 V). EMG response derived from three subjects as indicated. (B) (i) Magnetic resonance microscopy images of the spinal cord and the complex peripheral rim composed of posterior and anterior roots shown in cross-sections at spinal cord segmental levels as indicated (Calabrese et al., 2018). (ii) Estimated positions of the left T12–S2 posterior roots reflecting their complex anatomical arrangement (Wall et al., 1990).

the L4–S2 segments. Thus, the categorization based on the thresholds of the L2–L4 innervated RF and the L5–S2 innervated TS produced statistically separate rostrocaudal distributions of cathode positions with dispersions that almost perfectly matched the respective rostrocaudal segmental innervations in the anatomical model.

We further divided the RF-bias category into two sub-categories: RF bias_{noTS}, RF but not TS recruited even with maximum stimulation amplitude; and RF bias_{RF&TS}, RF and TS recruited. Between categories (Figure 3B), thresholds of RF and TS responses, respectively, differed significantly (datasets obtained with voltage-controlled stimulators, see Transparent Methods; Kruskal-Wallis tests; RF, $\chi^2(3) = 88.643$, $p < .001$, $r = .471$; TS, $\chi^2(2) = 84.299$, $p < .001$, $r = .483$). Post-hoc comparisons revealed significantly higher RF thresholds in the RF-bias_{noTS} category compared with any other category as well as significantly higher TS thresholds in the RF-bias_{RF&TS} category compared with the non-selective and the TS-bias categories (all $p < .001$). Response thresholds hence increased when progressively shifting cathode sites rostrally from the respective segmental innervations. Thresholds of RF and TS differed both within the RF bias_{RF&TS} category (Wilcoxon test; $Z = -13.223$, $p < .001$, $r = .878$) as well as within the TS bias category ($Z = -7.696$, $p < .001$, $r = .555$).

We expanded the analysis of response thresholds to all five studied muscles by fitting separate linear mixed models to the data obtained for each category (Figure 3C). No differences between thresholds were found for the RF-bias_{noTS} ($F(2,105) = .141$, $p = .869$, $\eta_p^2 = .003$; only thigh muscles compared), the non-selective ($F(4,411) = .924$, $p = .450$, $\eta_p^2 = .009$), nor the TS-bias categories ($F(4,194) = 2.237$, $p = .066$, $\eta_p^2 = .044$). In the RF-bias_{RF&TS} category, thresholds differed significantly ($F(4,1034) = 66.706$, $p < .001$, $\eta_p^2 = .205$). Post-hoc comparisons revealed lower thresholds for the thigh than the lower leg muscles (all $p < .001$). Notably,

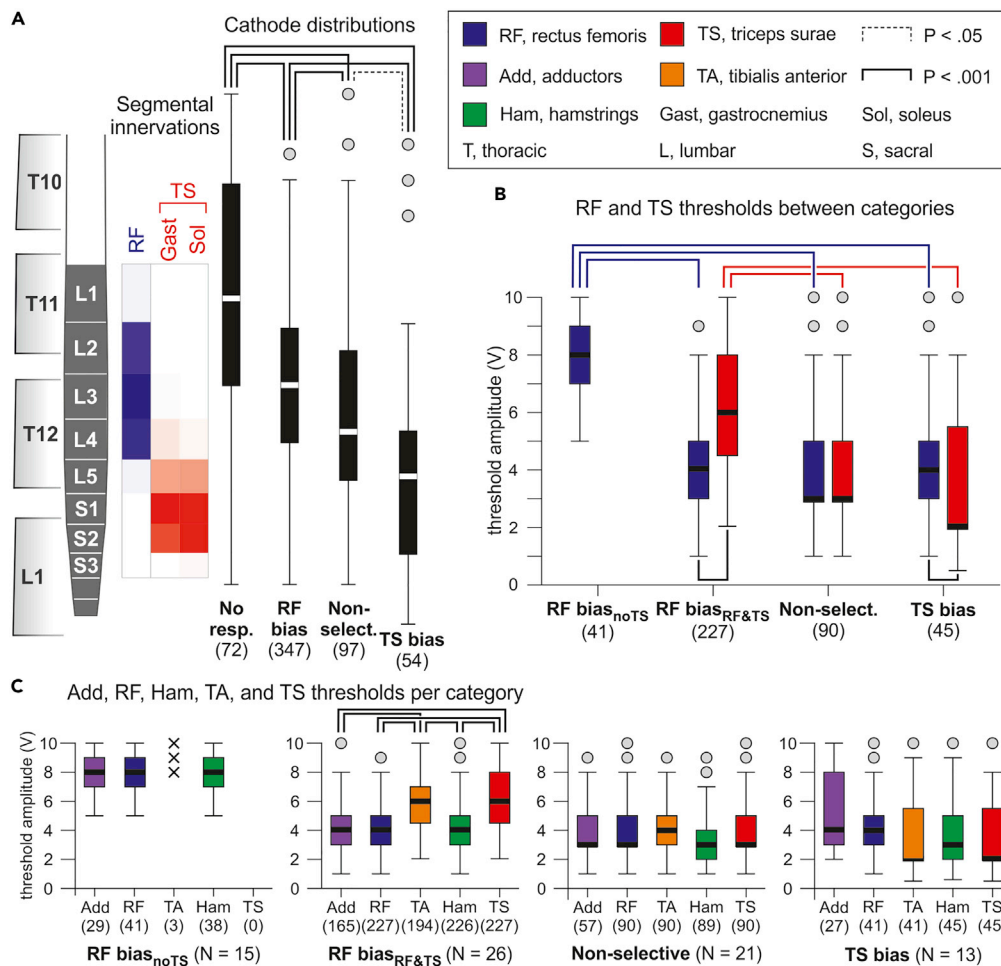


Figure 3. PRM-reflex thresholds of RF and TS reflect the segmental lumbosacral spinal cord anatomy

(A) Statistical comparison (Kruskal-Wallis test) of cathode distributions separated according to the elicitation of RF- and TS-PRM reflexes and their thresholds (Th). Categories are as follows: No RF and TS responses; RF bias, $Th_{RF} < Th_{TS}$; Non-selective, $Th_{RF} = Th_{TS}$; TS bias, $Th_{RF} > Th_{TS}$. Segmental innervation probabilities are illustrated by the opacity of blue (RF) and red (TS) boxes aligned with the spinal cord model. Data derived from all 34 subjects.

(B) Th_{RF} and Th_{TS} of the different categories; the RF-bias category was sub-divided into RF bias_{noTS}, RF but not TS recruited, and RF bias_{RF&TS}, RF and TS recruited. Statistical comparisons between categories were performed using Kruskal-Wallis test and within categories, using separate Wilcoxon tests.

(C) Response thresholds of Add, RF, TA, Ham, and TS per category. In the RF-bias_{noTS} category, TA responded in three cases only (x) and was not considered in the statistical comparison (linear mixed model). Numbers in parentheses are available datasets per category and muscle; N is the number of subjects per analysis. Boxplots illustrate median cathode locations (A) and response thresholds (B and C), respectively, as bold horizontal lines within boxes spanning the IQR, and whiskers extending to the smallest and largest values that are not outliers (values 1.5–3 times the IQR; plotted as circles). Brackets indicate statistical significance, dotted lines, $p < .05$, and solid lines, $p < .001$.

responses of Ham did not reflect the segmental innervation of this muscle group. Their thresholds differed neither from the RF thresholds in the two RF-bias categories nor from the TS threshold in the TS-bias category.

Finally, we compared the datasets obtained in the SCI (N = 26; number of datasets n = 319; see [Transparent Methods](#)) and the non-SCI subjects (N = 8; n = 179). There was a significant association between category (no responses, RF bias, non-selective, TS bias) and pathology (SCI, non-SCI), $\chi^2(3) = 11.113$, $p = .011$, Cramer's V = .149, with the SCI subjects contributing more (adjusted residuals of 2.2) than expected under the null hypothesis to the non-selective category and less (−2.6) to the no-responses category. Yet, there was

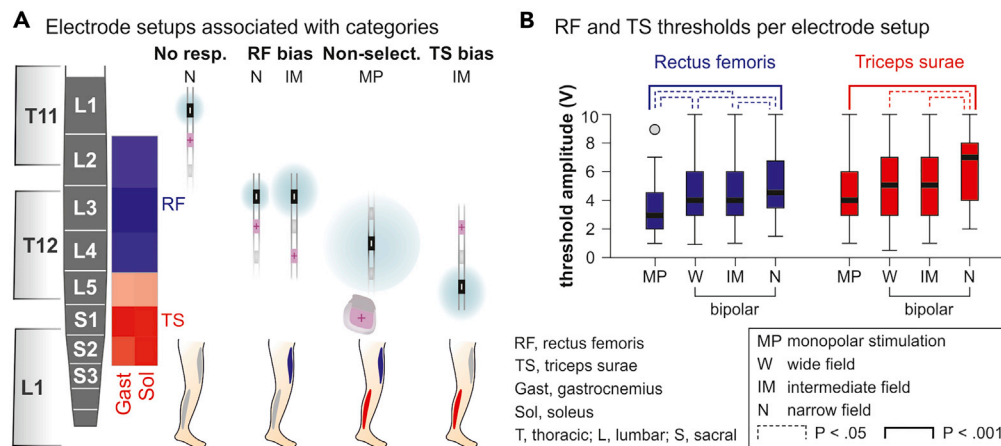


Figure 4. Impact of mono- and bipolar stimulation on selectivity and threshold of PRM-reflex elicitation

(A) Electrode setups contributing more than expected under the null hypothesis to the no-responses, RF-bias, non-selective, and TS-bias categories. Cathode (–) positions represent the medians of distributions within the four different categories, cf. Figure 3A, shown with respect to the major segmental innervations of RF and TS. Anodes (+) shield the distribution of the cathodic field (symbolized by blue areas).

(B) Dependence of RF- and TS-response thresholds on the electrode setup. Boxplots illustrate median thresholds as bold horizontal lines within boxes spanning the IQR and whiskers extending to the smallest and largest values that are not outliers (values 1.5–3 times the IQR; plotted as circle). Data derived from, monopolar stimulation, ten subjects; wide field, 30 subjects; intermediate field, 18 subjects; and narrow field, 14 subjects. Brackets indicate statistical significance (Kruskal-Wallis tests), dotted lines, $p < .05$, and solid lines, $p < .001$.

also a significant association between rostrocaudal cathode distribution (categorized into intervertebral disc or upper, middle, or lower third of vertebral body) and pathology ($\chi^2(14) = 88.344$, $p < .001$, Cramer's $V = .421$). When analyzing reduced datasets (SCI, $n = 232$ datasets; non-SCI, $n = 127$) with no statistical difference in cathode distribution between subject groups ($\chi^2(7) = 12.198$, $p = .094$, Cramer's $V = .184$), there was no association between category and pathology ($\chi^2(3) = 3.517$, $p = .319$, Cramer's $V = .099$).

Influence of cathode-anode setup

We found a significant association between electrode setup (bipolar stimulation with cathodes either rostral or caudal to anodes and with wide, intermediate, and narrow fields, or monopolar stimulation; see Transparent Methods) and the four RF- and TS-threshold-based categories ($\chi^2(24) = 61.491$, $p < .001$, Cramer's $V = .173$). Narrow fields with rostral cathodes contributed more (adjusted residual of 2.7) and monopolar setups less (–2.2) than expected under the null hypothesis to the no-responses category. Narrow and intermediate fields with rostral cathodes contributed more than expected to the RF-bias category (2.9 and 2.2, respectively), whereas intermediate fields with caudal cathodes contributed less (–2.7). Monopolar setups contributed more (2.2) and wide fields with rostral cathodes less (–2.1) than expected to the non-selective category. Intermediate fields with caudal cathodes contributed more than expected (2.4) to the TS-bias category. Figure 4A illustrates all electrode setups that contributed more than expected to a specific category. Thresholds of RF and TS, respectively, differed significantly between bipolar wide, intermediate, and narrow fields as well as monopolar stimulation (Kruskal-Wallis tests; RF, $\chi^2(3) = 25.701$, $p < .001$, $r = .241$; TS, $\chi^2(3) = 21.403$, $p < .001$, $r = .243$). Post-hoc comparisons revealed lower RF-thresholds for monopolar than for bipolar stimulation, as well as lower TS-thresholds for monopolar than bipolar stimulation with narrow fields; further significant differences are highlighted in Figure 4B.

Mapping of the lumbosacral spinal cord based on PRM-reflex amplitudes

We analyzed the peak-to-peak amplitudes of PRM reflexes at threshold (lowest stimulation amplitude evoking either RF or TS responses), common threshold (evoking RF and TS responses), as well as the maximum stimulation applied. For each electrode setup and stimulation amplitude, we obtained mean peak-to-peak amplitudes for each muscle per leg from all available responses and normalized them to the maximum mean peak-to-peak amplitude in the respective muscle obtained across all tested electrode setups in the same recording. Median values per muscle were then determined separately for the RF-bias,

the non-selective, and TS-bias categories and within each category for the three stimulation levels (394 datasets derived from 25 subjects; see [Transparent Methods](#)). Rostrocaudal cathode distributions differed significantly between categories also for this reduced number of datasets (Kruskal-Wallis test, $\chi^2(4) = 203.663$, $p < .001$, $r = .439$, all post-hoc pairwise comparisons $p < .001$).

Spinal cord maps of motoneuron pool activation derived from the RF- and TS-response amplitudes and segmental innervation probabilities showed a clear dependence on the rostrocaudal cathode sites ([Figure 5A](#)). A median cathode site at the L3 segmental level led to the selective activation of the L2–L4 spinal cord segments at threshold, with gradual spread to L5–S2 at common threshold and maximum stimulation amplitude, but the rostral segments remained predominantly activated. Conversely, a median cathode site at the S2 segmental level led to the selective activation of the L5–S2 spinal cord segments at threshold and recruited rostral segments with increased stimulation amplitudes. A median cathode site right between the segmental innervations of RF and TS resulted in a non-selective activation of L2–S2. Thus, threshold responses reflected the anatomical locations of the key segments of RF and TS, but increasing the stimulation amplitude led to a dissociation between the segmental cathode site and the activated spinal cord segments.

Polar plots of normalized response amplitudes reveal the preferential activation of the medial and anterior thigh muscles with a median cathode site at the L3 segmental level and of the lower-leg muscles with a median cathode site at S2 ([Figure 5B](#)). At maximum stimulation, the polygon function approached the shape of a regular pentagon in the non-selective category, indicating near equal recruitment of all muscles with a median cathode site between the L4 and L5 segmental levels. Ham was strongly recruited by all three cathode distributions.

We compared the normalized response amplitudes of the five muscles at common threshold and found significant differences in all three categories (linear mixed models; RF bias, $F(4,1085) = 366.725$, $p < .001$, $\eta_p^2 = .575$; non-selective, $F(4,322) = 18.488$, $p < .001$, $\eta_p^2 = .187$; and TS bias, $F(4,171) = 29.681$, $p < .001$, $\eta_p^2 = .410$). Significant results of post-hoc comparisons are shown in [Figure 5C](#). The segmental anatomy of the lumbosacral spinal cord was well reflected by the normalized EMG amplitudes of the PRM reflexes of Add, RF, TA, and TS, but not of Ham.

To investigate whether the type of upper motoneuron disorder would impact the PRM-reflex recruitment, we compared the EMG amplitudes obtained in the SCI ($N = 19$) and the non-SCI subjects ($N = 6$) within the RF-bias category, separately for threshold, common threshold, and maximum stimulation (statistical comparisons in other categories not possible due to sample sizes). At threshold and common threshold, no differences between the two subgroups were detected for any of the five muscles studied. At maximum stimulation, the EMG amplitudes of the Ham responses were larger in the SCI ($1579.6 \pm 163.2 \mu\text{V}$) than the non-SCI subjects ($889.4 \pm 289.7 \mu\text{V}$). Notably, absolute stimulation amplitudes did not differ between SCI and non-SCI subjects at threshold, common threshold, and maximum stimulation. The same analyses conducted for the severity of SCI (motor-complete, AIS A or B, $N = 13$; versus motor-incomplete, AIS C or D, $N = 6$) revealed no differences at threshold and common threshold. At maximum stimulation, EMG amplitudes of TA (motor-complete SCI: $451.6 \pm 72.0 \mu\text{V}$; motor-incomplete SCI: $154.2 \pm 103.6 \mu\text{V}$) and Ham responses ($1858.2 \pm 195.1 \mu\text{V}$; $1023.9 \pm 280.8 \mu\text{V}$) differed significantly. Again, stimulation amplitudes did not differ between subgroups. All values and results of the statistical testing are specified in [Tables S7](#) and [S8](#).

Intraoperative monitoring predicts postoperative segmental cathode position

The surgical placement of an epidural lead is guided by neurophysiological monitoring with the patient in the prone position, whereas postoperatively, the active electrodes along the epidural array are selected in the supine position ([Harkema et al., 2011](#); [Wagner et al., 2018](#)). We therefore tested whether segmental cathode positions and motoneuron pool activation identified intraoperatively would be maintained despite the considerable anterior-to-posterior migration of the spinal cord and roots within the dural sac accompanying the change in body position ([Holsheimer et al., 1994](#); [Ranger et al., 2008](#)). We analyzed 82 available pairs of datasets with the same electrode setups tested both intra- and postoperatively in a given subject ([Figure 6A](#)). Statistical testing revealed a significant association between categories ($\chi^2(16) = 79.975$, $p < .001$, Cramer's $V = .494$; [Figure 6B](#)). The following transitions occurred more frequently than expected under the null hypothesis: RF bias_{noTS, prone} to RF bias_{RF&TS, supine} (adjusted residual: 2.7); RF bias_{RF&TS, prone} to RF bias_{RF&TS, supine} (3.1); non-selective_{prone} to non-selective_{supine} (3.1); TS bias_{prone} to TS

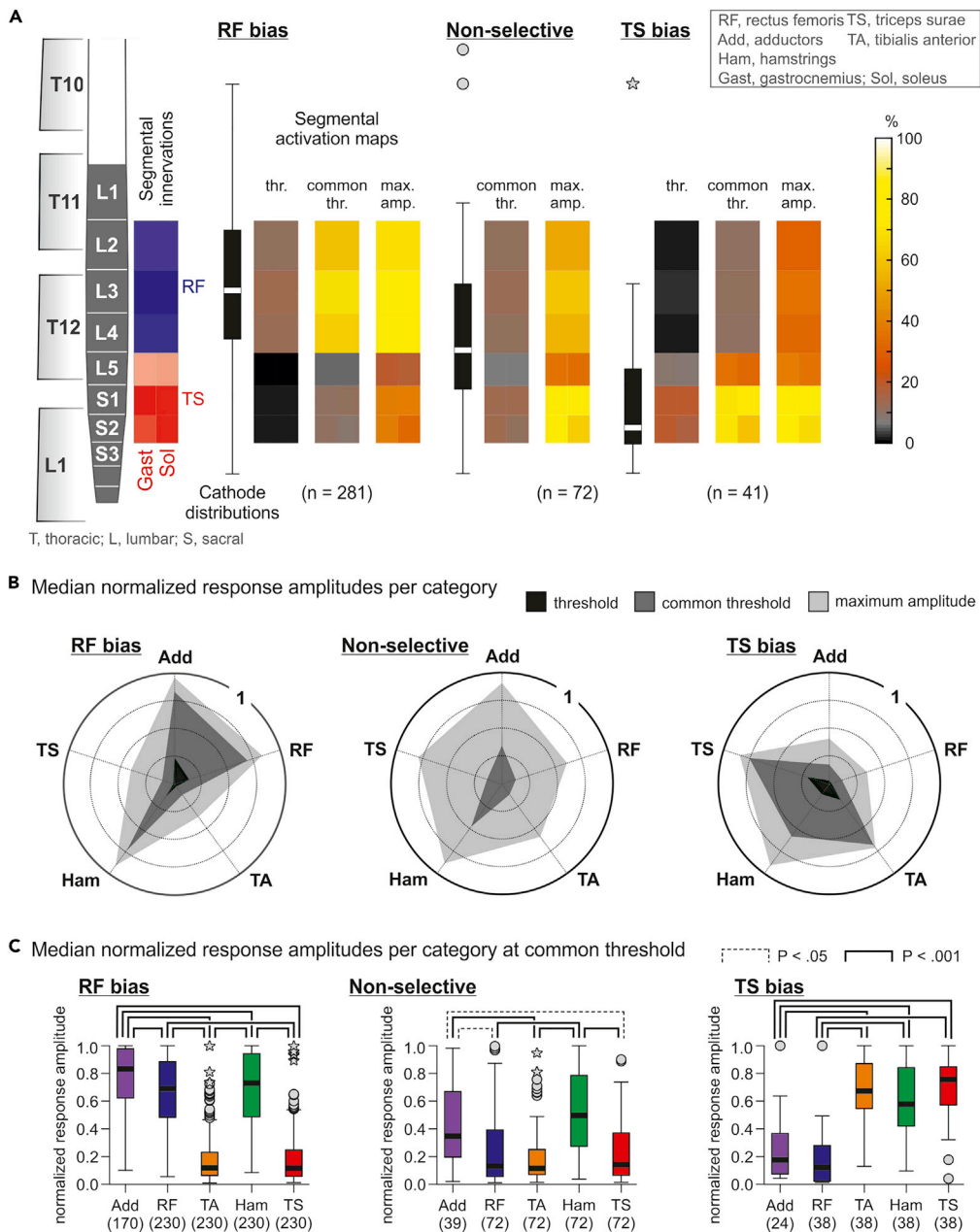


Figure 5. PRM-reflex amplitudes reflect the segmental lumbosacral spinal cord anatomy

(A) Spinal cord maps of spatial motoneuron pool activation for three cathode distributions (RF bias, non-selective, TS bias) and three stimulation-amplitude levels (threshold, common threshold, maximum) derived from normalized response amplitudes and segmental innervation probabilities. Only major segmental innervations of RF and TS (innervation probabilities $\geq 44\%$; Figure 1C) were considered, illustrated by the opacity of blue and red boxes. Data derived from 25 subjects.

(B) Polar plots of muscle activation for the three categories and stimulation levels. Radial axes are muscles and polar coordinates are median normalized peak-to-peak amplitudes.

(C) Normalized response amplitudes of all muscles studied per category at common threshold and compared using separate linear mixed models. Numbers in parentheses are available datasets per category and muscle. Boxplots illustrate median cathode locations (A) and response thresholds (C), respectively, as bold horizontal lines within boxes spanning the IQR, and whiskers extending to the smallest and largest values that are not outliers (values 1.5–3 times the IQR; plotted as circles) or extreme values (values >3 times the IQR; asterisks). Brackets indicate statistical significance, dotted lines, $p < .05$, and solid lines, $p < .001$.

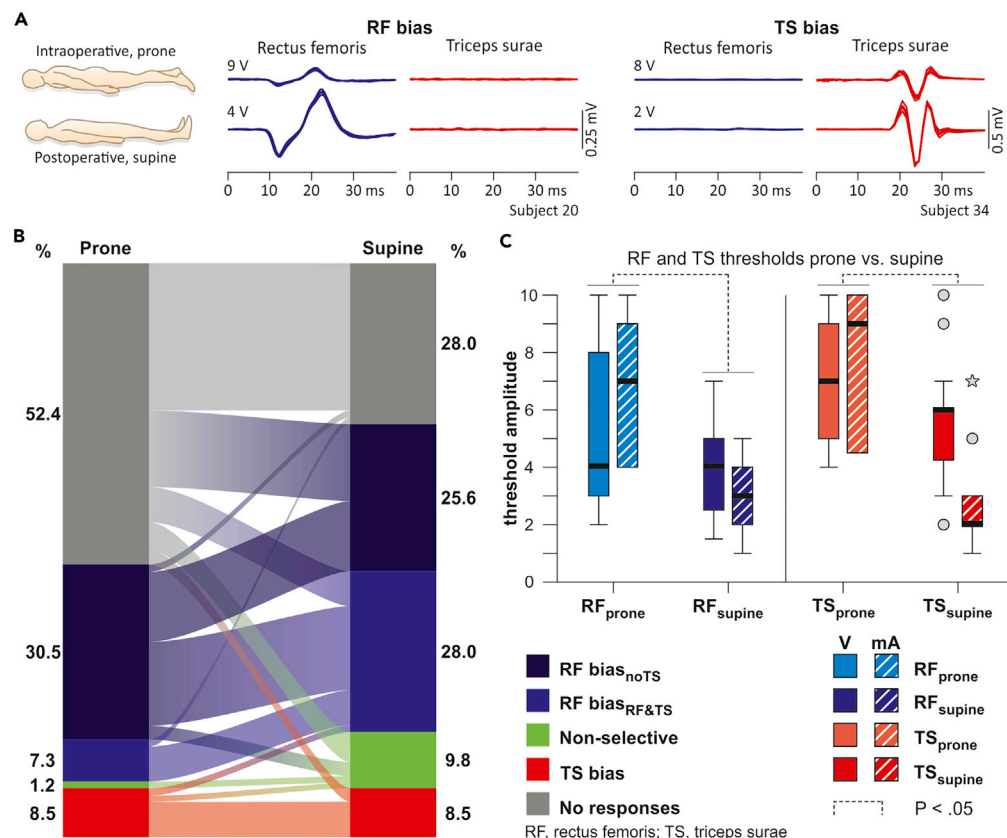


Figure 6. Intraoperative monitoring predicts postoperative segmental motoneuron pool activation

(A) EMG recordings of PRM reflexes evoked in RF and TS at threshold, intraoperatively in the prone and postoperatively in the supine position; five superimposed responses each. RF- versus TS-selectivity of the stimulation intraoperatively was maintained postoperatively, with decreased thresholds.

(B) Transitions between categories from the prone to the supine position. Eighty-seven percent of the intraoperative datasets that were classified into either of the two RF-bias categories and 71% of those of the TS-bias category remained within the respective categories postoperatively. Data derived from 16 subjects.

(C) Thresholds of RF and TS responses evoked in the prone and supine positions. Data derived from 12 subjects.

Thresholds for voltage- and current-controlled stimulators were pooled for the statistical testing, because pairwise comparisons were based on signed ranks (Wilcoxon test). Boxplots illustrate median thresholds as bold horizontal lines within boxes spanning the IQR and whiskers extending to the smallest and largest values that are not outliers (values 1.5–3 times the IQR; plotted as circles) or extreme values (values >3 times the IQR; asterisks). Brackets (dotted lines) indicate statistical significance, $p < .05$.

$\text{bias}_{\text{supine}}$ (6.2); and no responses_{prone} to no responses_{supine} (4.4). Transitions from RF bias_{noTS, prone} to no responses_{supine} (−3.2) and no responses_{prone} to RF bias_{RF&TS, supine} (−3.5) occurred less frequently than expected.

In 37 of the 82 data pairs, RF and TS were recruited in the prone as well as the supine position and allowed the statistical comparison of response thresholds between body positions (Figure 6C). Pairwise comparisons revealed higher thresholds in the prone than the supine position for the recruitment of both muscles (Wilcoxon tests; RF, $Z = -3.336$, $p = .001$, $r = .599$; TS, $Z = -2.524$, $p = .012$, $r = .700$). Intraoperative segmental mapping hence predicted the segmental motoneuron pool activation obtained postoperatively with reduced response thresholds in the supine position.

Laterally located electrodes can lead to a dissociation between segmental cathode sites and activated spinal cord segments

We had hypothesized that midline-located electrodes would map the segmental organization of the lumbosacral spinal cord by preferentially activating posterior roots at their segmental entries (Capogrosso

et al., 2013; Ladenbauer et al., 2010; Rattay et al., 2000; Struijk et al., 1993) and hence recruit motoneuron pools at the location of the stimulating cathode. Laterally placed electrodes could be located closer to posterior roots of passage and therefore activate more rostral spinal cord segments at threshold (Figure S3A). We explored this assumption by comparing pairs of datasets with midline and lateral electrode leads with same rostrocaudal anode and cathode positions (available from three subjects; see Data S1). For all midline-located bipolar electrode setups at the T12 vertebral level ($n = 27$), 66.7% of the datasets were classified into either of the two RF-bias categories, all of which remained within these categories when stimulation was shifted laterally (Figure S3B). Additional contributions from the non-selective and no-responses categories resulted in overall 77.8% of the datasets to belong to the RF-bias categories for lateral stimulation, hence increasing L2–L4 selectivity. For all midline-located bipolar electrode setups at the L1 vertebral level ($n = 22$), 27.3% of the datasets were classified into the TS-bias category, of which 83.3% changed to one of the two RF-bias categories and another 16.7% to the no-responses category with laterally located electrodes. None of the datasets were classified into the TS-bias category with lateral stimulation.

Discussion

We mapped the spinal cord through EES of a complex interface—the lumbosacral posterior roots floating in the cerebrospinal fluid. Classifying cathode locations according to relative thresholds of RF and TS responses resulted in separate rostrocaudal spatial dispersions that near-perfectly matched the statistically predicted anatomical locations of the respective motoneuron pools. EMG amplitudes of Add, RF, TA, and TS responses reflected the segmental organization of the spinal cord, but Ham was an exception. Theories on low-threshold sites of posterior root fibers and the impact of mono- and bipolar stimulation were confirmed. Motor recruitment by EES was directly compared between subjects with traumatic SCI and other upper motoneuron disorders for the first time. Differences were present at maximum stimulation amplitudes. Postoperative selectivity of motoneuron pool activation by EES in supine was predictable from intraoperative recordings in the prone position.

To estimate segmental cathode positions, we constructed the—to our knowledge—most comprehensive statistical model of the spine and spinal cord published to date. To mitigate inaccuracies in our interpretations resulting from the variability of anatomical parameters, our model integrated data from thousands of subjects and 59 sources. In addition, our cohort of 34 subjects was the largest in contemporary studies of EES in motor disorders. The termination level of the conus medullaris was an essential parameter, because its variation directly results in a shift of the vertebral positions of spinal cord segments (Wall et al., 1990). The deviation of the mean termination level of our sample from the population median was estimated to be less than 6 mm, with a confidence of 95%. The goodness of representation of our sample by the population model was reflected by the near-perfect match of the mapping results of RF and TS and the estimated anatomical locations of the L2–L4 and L5–S2 spinal cord segments. Our population model constructed by stacking spinal cord segmental heights is in good agreement with the vertebral positions of the lumbosacral spinal cord found in anatomical studies of human cadavers, which identified the rostral border of the L1 segment at the upper third of the T11-vertebral body and that of the S1 segment at the lower endplate of the T12 or the upper endplate of the L1-vertebral body (Canbay et al., 2014; Hintzsche and Gisler, 1935; Lang and Geisel, 1983; Wall et al., 1990). The major variations were the exact locations of the individual lumbar spinal cord segments. A recent study constructed an anatomical model of the C2–L5 spinal cord segments in relationship to bony landmarks using multiple parameters measured in nine human cadavers (Mendez et al., 2020). Compared with our model, the rostral border of the L1 spinal cord segment was near-identical, but the entire lumbar spinal cord was stretched in caudal direction by approximately 20%. This difference may stem from the different assumptions used to construct the models, e.g., the correlation between vertebral bone height and the intervertebral foramen-to-dorsal root entry zone distance used in (Mendez et al., 2020).

The vast majority of EES applications is in pain control and is firmly associated with the antidromic activation of sensory dorsal column fibers (Gildenberg, 2009). Sensory effects and evoked muscle responses might however be initiated separately in dorsal columns and posterior roots, respectively (He et al., 1994; North et al., 1997). In cats and non-human primates, the majority of long dorsal column fibers ascending from the lumbosacral to the thoracic and cervical spinal cord come from cutaneous mechanoreceptors (Davidoff, 1989). The ascending projections from hindlimb muscle spindle afferents largely terminate in the upper lumbar and lower thoracic segments, supposedly occupying deep positions in the dorsal

columns to make synaptic contact with the posterior gray column/Clarke's column (Brodal, 1981; Lloyd and McIntyre, 1950; Whitsel et al., 1969). This may be the case in humans as well (York, 1985). Neural structures activated by EES are limited to the largest-diameter myelinated fibers in the outermost layer of the dorsal columns and to the posterior roots (Holsheimer, 1998, 2002). Posterior root fibers have lower thresholds (Capogrosso et al., 2013; Rattay et al., 2000; Struijk et al., 1993), largely because of the electrical conductivity of the cerebrospinal fluid (Geddes and Baker, 1967), which channels 80%–90% of the injected current flow (Holsheimer, 1998; Ladenbauer et al., 2010). The lumbar and upper sacral posterior roots hold all muscle spindle fibers from the lower extremities (Brodal and Rinvik, 1981; Lloyd, 1943). Our results strongly support that the evoked responses were not related to dorsal column stimulation, because statistically, response thresholds increased when stimulating cathode locations were rostral to the respective segmental posterior root entries. By contrast, responses could be evoked in a muscle when cathodes were located over the longitudinal extent of the associated posterior roots, i.e., at the segments of their homonymous motoneuron pools and caudally along the entire length of the terminal spinal cord (note that the vertebral exit levels of the L2–S2 roots are all caudal to the spinal cord termination level). Together with the demonstration of their reflex nature (see Data S1 and Figure S2), as in previous studies (Hofstoetter et al., 2018; Minassian et al., 2004, 2016), we confirmed that all evoked responses analyzed here were PRM reflexes.

Previous electrophysiological studies had employed stimulation of posterior or anterior roots with the aim to identify the segmental innervation probabilities of lower-extremity muscles (Phillips and Park, 1991; Schirmer et al., 2011; Thage, 2009). Anatomically isolated roots exposed during surgery were directly stimulated, with current spread to other roots effectively avoided. In the present study, we mapped the segmentally organized motoneuronal pool activity of the L2–S2 spinal cord *indirectly* through electrical stimulation applied from the epidural space with inevitable current spread within the cerebrospinal fluid (Capogrosso et al., 2013) and concomitant depolarization of multiple posterior roots (Rattay et al., 2000) with complex topographic anatomy (Wall et al., 1990). The L3 spinal cord segment is flanked by the L3–T12 roots, and the S2 segment by the S2–L1 roots (Figure 2B). Posterior roots of passage from rostral segments are located laterally and, at sacral spinal cord levels, they additionally start to overlap in a posterior-anterior fashion so that the S1 posterior roots overlay the other sacral roots (Wall et al., 1990). The posterior roots may thus pose a barrier and reduce the current flow not only to the dorsal columns but also to other roots. Despite this complexity and the fact that posterior roots can be stimulated along their entire length, muscles with separate segmental innervations were selectively recruited by cathodes located over the respective spinal cord segments. This selectivity can be explained by low-threshold sites of posterior root fibers at their entries into the spinal cord proposed by computer modeling studies (Ladenbauer et al., 2010; Rattay et al., 2000; Struijk et al., 1993). The present results may be the first practical demonstration of this long-assumed theory. Increased stimulation amplitudes caused a dissociation between the segmental cathode sites and the activated spinal cord segments. For cathodes over the lumbar spinal cord, this dissociation likely resulted from longitudinal current spread additionally recruiting the caudally located sacral roots and for cathodes over the sacral spinal cord, from transversal current spread around the spinal cord additionally recruiting the laterally located lumbar roots (Minassian et al., 2007; Rattay et al., 2000; Wall et al., 1990).

Computational modeling had predicted that monopolar stimulation would result in lower thresholds for posterior root stimulation, whereas bipolar setups would have a higher spatial selectivity (Struijk et al., 1993). Here, we demonstrated that thresholds of RF- and TS-PRM reflexes were lower for monopolar than bipolar stimulation. Concurrently, monopolar stimulation contributed more than statistically expected to the non-selective recruitment of RF and TS, whereas bipolar setups were more likely to recruit either of these muscles selectively. Computer simulations had also described an influence of the relative anode position in bipolar setups, with the anode shielding neural structures from cathodal stimulation (Rattay et al., 2000; Struijk et al., 1993). Our data showed that bipolar stimulation with caudal anodes contributed more than expected to the selective recruitment of RF, whereas the opposite polarity contributed more to a TS-biased recruitment.

There is a common consensus that epidural electrode arrays implanted for enhancing lower-extremity motor function need to overlay the lumbar and upper sacral spinal cord segments (Angeli et al., 2018; Gill et al., 2018; Wagner et al., 2018). Importantly, our data revealed that stimulation that was selective for either the mid-lumbar or upper sacral spinal cord during intraoperative monitoring in the prone position remained

selective during postoperative studies in the supine position despite the considerable anterior-to-posterior migration of the spinal cord and roots when changing body position (Holsheimer et al., 1994; Ranger et al., 2008). This is relevant, because optimization of electrode configurations and stimulation parameters postoperatively is conducted in the supine position. In line with the spinal cord and roots moving closer to the posteriorly located epidural electrodes (Holsheimer et al., 1994), stimulation thresholds dropped in the supine position.

Our mapping study based on the use of midline-located, percutaneous linear electrode leads. Recent studies applying EES for the recovery of lower-extremity motor function had employed surgical paddle arrays with 16 electrodes arranged in three columns (Calvert et al., 2019a; Grahn et al., 2017; Harkema et al., 2011), although few investigations have capitalized on lateral cathodes to enhance motor function in the ipsilateral lower extremity (Gill et al., 2018; Wagner et al., 2018). Our results recommend that the identification of segmental cathode locations should be primarily performed using midline-located electrode setups. Laterally located electrodes may activate posterior roots of passage and activate spinal segments that do not correspond to the rostrocaudal stimulation site.

We used the lowest programmable EES frequency to ensure a relationship between segmental stimulation sites and activated spinal cord segments given by homonymous monosynaptic connections (Capogrosso et al., 2013; Minassian et al., 2004). The resulting spinal mapping represents an essential step toward establishing a framework of the causal relationship between epidural stimulation site, electrode setup, stimulation amplitude, and the recruited posterior roots. The impact of EES frequency requires an in-depth analysis to complement this framework. Functionally, variation of EES frequency may be exploited to alter the balance of activation between recruited motoneuron pools. An increase of EES frequency from 5–16 Hz to 21 Hz and beyond was suggested to shift the motor output patterns to flexor muscles (Jilge et al., 2004; Wagner et al., 2018). Indeed, mid-lumbar posterior-root stimulation at frequencies of 60 to 120 Hz could evoke a synergistic activation of flexor muscles that was used to facilitate the swing phase during over-ground locomotion in individuals with SCI (Wagner et al., 2018).

Limitations of the study

Our analysis involved the pooling of EMG data obtained by different electrode setups. We stratified for monopolar and bipolar stimulation and within the bipolar subset of data, for different setups. Differences in impedance across electrodes and subjects could have additionally influenced PRM-reflex recruitment. Electrode dimensions and materials of all lead models used were the same, leaving the conductor wire resistance as the only difference between models (Device specifications for lead models, Medtronic). Excluding this resistance, the median bipolar tissue impedance (Model 3487A) was previously measured to be 547 Ω (IQR: 453–652 Ω) (Alò et al., 2006). An increase in tissue impedance caused by fibrous encapsulation is a late phenomenon, not occurring within 18 days post-implantation (Alò et al., 2006), and was likely not relevant here. Tissue impedance can also increase should the stimulating electrodes not directly contact the dura mater (Manola and Holsheimer, 2004). Using voltage-controlled stimulators and monopolar or bipolar EES, alterations in impedance will change the current amplitudes in an inversely proportional way but will have little influence on the current flow directions within the dural sac (Manola and Holsheimer, 2004). Thus, these factors may shift the absolute response thresholds rather than change the recruitment order of spinal cord segments.

We focused parts of our analysis on RF and TS responses because among the tested muscles, their motoneuron pools show the least segmental overlap, which was essential for our threshold-based approach to identify segmental cathode locations. We might have used Add instead of RF; however, data of Add responses were available only in 25 subjects. Add was not considered in other EES studies (Angeli et al., 2018; Gill et al., 2018; Harkema et al., 2011; Wagner et al., 2018). An electrode lead placed to cover the L2–S2 segments can be configured to recruit all muscles essential for locomotion. Optimally targeting the hip flexor muscles may require electrodes located more rostrally by one segment (Wagner et al., 2018). As opposed to the noninvasive assessment employed here, selective EMG recordings from the deeply located iliopsoas muscle require fine-wire electrodes (Angeli et al., 2014; Harkema et al., 2011), or intraoperatively, intramuscular needle electrodes (Wagner et al., 2018).

All data were collected from participants being treated for spasticity, which could have led to excitability changes of monosynaptic reflex connections and thus impact the recruitment of PRM reflexes. PRM

reflexes share some physiological characteristics with the H reflex (Minassian et al., 2020). Conflicting information exists regarding changes in the H reflex threshold and gain (slope of the H-reflex recruitment curve) in chronic SCI, proposed to be lower, equal, as well as higher compared with controls (Hilgevoord et al., 1994; Knikou et al., 2009; Schindler-Ivens and Shields, 2004). In the case of increased reflex excitability, the activation of a relatively small fraction of afferents could be sufficient to elicit a PRM reflex. Thus, the effective range of an epidural cathode would be increased and the segmental specificity reduced. Should such excitability changes be muscle specific, they could partially explain the behavior of Ham, as threshold stimulation did not reflect its segmental innervation. Our data suggest that PRM reflexes of Ham would not provide useful information for intraoperative monitoring to guide epidural lead placement.

We had included data of subjects with heterogeneous types of upper motoneuron disorders and severities of traumatic SCI in order to map the lumbosacral spinal cord from a wide range of available rostrocaudal cathode positions and to increase the sample size for intra- and postoperative comparisons with appropriate statistical power. This heterogeneity had no confounding impact on the major results of our study because there were no statistical differences in PRM recruitment between the subgroups at threshold and common threshold. Our results may suggest that individuals with upper motoneuron disorders other than SCI could be recruited for future studies of EES for motor recovery with similar effects on lower-extremity motor recruitment to be expected.

Resource availability

Lead contact

Further information and requests should be directed to and will be fulfilled by the Lead Contact, Ursula Hofstoetter (ursula.hofstoetter@meduniwien.ac.at).

Materials availability

This study did not generate new materials or new unique reagents.

Data and code availability

The published article includes all datasets analyzed during this study. Data were analyzed using MATLAB R2019a, The MathWorks, Inc., Natick, MA, USA, and IBM SPSS Statistics 26.0 for Windows, IBM Corporation, Armonk, NY, USA.

Methods

All methods can be found in the accompanying [Transparent methods supplemental file](#).

Supplemental information

Supplemental Information can be found online at <https://doi.org/10.1016/j.isci.2020.101930>.

Acknowledgments

The study was supported by the Austrian Science Fund (FWF), proj.nr. I 3837-B34. We wish to acknowledge the continuous support by Prof. Wolfgang Drexler, Head of Center for Medical Physics and Biomedical Engineering, Medical University of Vienna, Austria.

Author contributions

Conceptualization: K.M. and U.S.H.; Methodology: U.S.H., I.P., and K.M.; Software: U.S.H. and I.P.; Analysis: U.S.H., I.P., and A.B.; Resources: P.L., H.B., and B.F.; Data Curation: B.F. and U.S.H.; Writing—Original Draft: U.S.H., I.P., and K.M.; Review & Editing: all authors; Visualization: U.S.H., I.P., and A.B.; Supervision: K.M. and B.F.; Funding Acquisition: U.S.H.

Declaration of interests

The authors declare no competing interests.

Received: July 16, 2020
Revised: October 6, 2020
Accepted: December 8, 2020
Published: January 22, 2021

References

- Air, E.L., Toczyl, G.R., and Mandybur, G.T. (2012). Electrophysiologic monitoring for placement of laminectomy leads for spinal cord stimulation under general anesthesia. *Neuromodulation* 15, 573–580.
- Alò, K., Varga, C., Krames, E., Prager, J., Holsheimer, J., Manola, L., and Bradley, K. (2006). Factors affecting impedance of percutaneous leads in spinal cord stimulation. *Neuromodulation* 9, 128–135.
- Angeli, C.A., Boakye, M., Morton, R.A., Vogt, J., Benton, K., Chen, Y., Ferreira, C.K., and Harkema, S.J. (2018). Recovery of over-ground walking after chronic motor complete spinal cord injury. *N. Engl. J. Med.* 379, 1244–1250.
- Angeli, C.A., Edgerton, V.R., Gerasimenko, Y.P., and Harkema, S.J. (2014). Altering spinal cord excitability enables voluntary movements after chronic complete paralysis in humans. *Brain* 137, 1394–1409.
- Barolat, G., Massaro, F., He, J., Zeme, S., and Ketcik, B. (1993). Mapping of sensory responses to epidural stimulation of the intraspinal neural structures in man. *J. Neurosurg.* 78, 233–739.
- Barolat, G., Singh-Sahni, K., Staas, W.E., Shatin, D., Ketcik, B., and Allen, K. (1995). Epidural spinal cord stimulation in the management of spasms in spinal cord injury: a prospective study. *Stereotact. Funct. Neurosurg.* 64, 153–164.
- Brodal, A. (1981). *Neurological Anatomy in Relation to Clinical Medicine*, Third edition (Oxford University Press).
- Brodal, P., and Rinvik, E. (1981). The somatic afferent pathways. In *Neurological Anatomy in Relation to Clinical Medicine*, A. Brodal, ed. (Oxford University Press), pp. 46–147.
- Calabrese, E., Adil, S.M., Cofer, G., Perone, C.S., Cohen-Adad, J., Lad, S.P., and Johnson, G.A. (2018). Postmortem diffusion MRI of the entire human spinal cord at microscopic resolution. *Neuroimage Clin.* 18, 963–971.
- Calvert, J.S., Grahn, P.J., Strommen, J.A., Lavrov, I.A., Beck, L.A., Gill, M.L., Linde, M.B., Brown, D.A., Van Straaten, M.G., Veith, D.D., et al. (2019a). Electrophysiological guidance of epidural electrode array implantation over the human lumbosacral spinal cord to enable motor function after chronic paralysis. *J. Neurotrauma* 36, 1451–1460.
- Calvert, J.S., Grahn, P.J., Zhao, K.D., and Lee, K.H. (2019b). Emergence of epidural electrical stimulation to facilitate sensorimotor network functionality after spinal cord injury. *Neuromodulation* 22, 244–252.
- Canbay, S., Güler, B., Bozkurt, M., Comert, A., Izcı, Y., and Başkaya, M.K. (2014). Anatomical relationship and positions of the lumbar and sacral segments of the spinal cord according to the vertebral bodies and the spinal roots. *Clin. Anat.* 27, 227–233.
- Capogrosso, M., Wenger, N., Raspopovic, S., Musienko, P., Beuparlant, J., Bassi Luciani, L., Courtine, G., and Micera, S. (2013). A computational model for epidural electrical stimulation of spinal sensorimotor circuits. *J. Neurosci. Off. J. Soc. Neurosci.* 33, 19326–19340.
- Cook, A.W., and Weinstein, S.P. (1973). Chronic dorsal column stimulation in multiple sclerosis. Preliminary Report. *N. Y. State J. Med.* 73, 2868–2872.
- Davidoff, R.A. (1989). The dorsal columns. *Neurology* 39, 1377–1385.
- Dimitrijevic, M.M., Dimitrijevic, M.R., Illis, L.S., Nakajima, K., Sharkey, P.C., and Sherwood, A.M. (1986). Spinal cord stimulation for the control of spasticity in patients with chronic spinal cord injury: I. Clinical observations. *Cent. Nerv. Syst. Trauma* 3, 129–144.
- Dimitrijevic, M.R., Faganel, J., Sharkey, P.C., and Sherwood, A.M. (1980). Study of sensation and muscle twitch responses to spinal cord stimulation. *Int. Rehabil. Med.* 2, 76–81.
- Formento, E., Minassian, K., Wagner, F., Mignardot, J.B., Le Goff-Mignardot, C.G., Rowald, A., Bloch, J., Micera, S., Capogrosso, M., and Courtine, G. (2018). Electrical spinal cord stimulation must preserve proprioception to enable locomotion in humans with spinal cord injury. *Nat. Neurosci.* 21, 1728–1741.
- Geddes, L.A., and Baker, L.E. (1967). The specific resistance of biological material—a compendium of data for the biomedical engineer and physiologist. *Med. Biol. Eng.* 5, 271–293.
- Gildenberg, P. (2009). Neuromodulation: a historical perspective. In *Neuromodulation*, P. Peckham, and A. Rezai, eds. (Elsevier-Academic Press), pp. 9–20.
- Gill, M.L., Grahn, P.J., Calvert, J.S., Linde, M.B., Lavrov, I.A., Strommen, J.A., Beck, L.A., Sayenko, D.G., Van Straaten, M.G., Drubach, D.I., et al. (2018). Neuromodulation of lumbosacral spinal networks enables independent stepping after complete paraplegia. *Nat. Med.* 24, 1677–1682.
- Grahn, P.J., Lavrov, I.A., Sayenko, D.G., Van Straaten, M.G., Gill, M.L., Strommen, J.A., Calvert, J.S., Drubach, D.I., Beck, L.A., Linde, M.B., et al. (2017). Enabling task-specific volitional motor functions via spinal cord neuromodulation in a human with paraplegia. *Mayo Clin. Proc.* 92, 544–554.
- Harkema, S., Gerasimenko, Y., Hodes, J., Burdick, J., Angeli, C., Chen, Y., Ferreira, C., Willhite, A., Rejc, E., Grossman, R.G., et al. (2011). Effect of epidural stimulation of the lumbosacral spinal cord on voluntary movement, standing, and assisted stepping after motor complete paraplegia: a case study. *Lancet* 377, 1938–1947.
- He, J., Barolat, G., Holsheimer, J., and Struijk, J.J. (1994). Perception threshold and electrode position for spinal cord stimulation. *Pain* 59, 55–63.
- Hilgevoord, A.A.J., Koelman, J.H.T.M., Bour, L.J., and Ongerboer de Visser, B.W. (1994). Normalization of soleus H-reflex recruitment curves in controls and a population of spastic patients. *Electroencephalogr. Clin. Neurophysiol. Potentials Sect.* 93, 202–208.
- Hintzsche, E., and Gisler, P. (1935). Die Lage der Rückenmarksegmente im Wirbelkanal. *Schweiz Arch. Neurol. Neurochir Psychiatr.* 35, 287–294.
- Hofstoetter, U.S., Freundl, B., Binder, H., and Minassian, K. (2018). Common neural structures activated by epidural and transcutaneous lumbar spinal cord stimulation: elicitation of posterior root-muscle reflexes. *PLoS One* 13, e0192013.
- Holsheimer, J. (2002). Which neuronal elements are activated directly by spinal cord stimulation. *Neuromodulation* 5, 25–31.
- Holsheimer, J. (1998). Computer modelling of spinal cord stimulation and its contribution to therapeutic efficacy. *Spinal Cord* 36, 531–540.
- Holsheimer, J., den Boer, J.A., Struijk, J.J., and Rozeboom, A.R. (1994). MR assessment of the normal position of the spinal cord in the spinal canal. *AJNR. Am. J. Neuroradiol.* 15, 951–959.
- Illis, L.S., Oygur, A.E., Sedgwick, E.M., and Awadalla, M.A. (1976). Dorsal-column stimulation in the rehabilitation of patients with multiple sclerosis. *Lancet (London, England)* 1, 1383–1386.
- Jilge, B., Minassian, K., Rattay, F., Pinter, M.M., Gerstenbrand, F., Binder, H., and Dimitrijevic, M.R. (2004). Initiating extension of the lower limbs in subjects with complete spinal cord injury by epidural lumbar cord stimulation. *Exp. Brain Res.* 154, 308–326.
- Knikou, M., Angeli, C.A., Ferreira, C.K., and Harkema, S.J. (2009). Soleus H-reflex gain, threshold, and amplitude as function of body posture and load in spinal cord intact and injured subjects. *Int. J. Neurosci.* 119, 2056–2073.
- Krames, E., Rezai, A., Peckham, P., and Aboelsaad, F. (2009). What is neuromodulation?, E.K. Neuromodulation, P. Peckham, and A. Rezai, eds. (Elsevier-Academic Press), pp. 3–8.
- Ladenbauer, J., Minassian, K., Hofstoetter, U.S., Dimitrijevic, M.R., and Rattay, F. (2010). Stimulation of the human lumbar spinal cord with implanted and surface electrodes: a computer simulation study. *IEEE Trans. Neural Syst. Rehabil. Eng.* 18, 637–645.

- Lang, J., and Geisel, U. (1983). [Lumbosacral part of the dural sac and the topography of its contents]. *Morphol. Med.* 3, 27–46.
- Lloyd, D. (1943). Neuron patterns controlling transmission of ipsilateral hind limb reflexes in cat. *J. Neurophysiol.* 6, 293–315.
- Lloyd, D.P.C., and McIntyre, A.K. (1950). Dorsal column conduction of group I muscle afferent impulses and their relay through Clarke's column. *J. Neurophysiol.* 13, 39–54.
- Manola, L., and Holsheimer, J. (2004). Technical performance of percutaneous and laminectomy leads analyzed by modeling. *Neuromodulation* 7, 231–241.
- Mendez, A., Islam, R., Latypov, T., Basa, P., Joseph, O., Knudsen, B., Siddiqui, A., Summer, P., Staehne, L., Grahm, P., et al. (2020). Segment-specific orientation of the dorsal and ventral roots for precise therapeutic targeting of human spinal cord. *bioRxiv* 31, 928804.
- Minassian, K., Freundl, B., and Hofstoetter, U. (2020). The posterior root-muscle reflex. In *Neurophysiology in Neurosurgery. A Modern Approach*, V. Deletis, J. Shils, F. Sala, and K. Seidel, eds. (Academic Press), pp. 239–253.
- Minassian, K., Hofstoetter, U., Tansey, K., and Mayr, W. (2012). Neuromodulation of lower limb motor control in restorative neurology. *Clin. Neurol. Neurosurg.* 114, 489–497.
- Minassian, K., Jilge, B., Rattay, F., Pinter, M.M., Binder, H., Gerstenbrand, F., and Dimitrijevic, M.R. (2004). Stepping-like movements in humans with complete spinal cord injury induced by epidural stimulation of the lumbar cord: electromyographic study of compound muscle action potentials. *Spinal Cord* 42, 401–416.
- Minassian, K., McKay, W.B., Binder, H., and Hofstoetter, U.S. (2016). Targeting lumbar spinal neural circuitry by epidural stimulation to restore motor function after spinal cord injury. *Neurotherapeutics* 13, 284–294.
- Minassian, K., Persy, I., Rattay, F., Pinter, M.M., Kern, H., and Dimitrijevic, M.R. (2007). Human lumbar cord circuitries can be activated by extrinsic tonic input to generate locomotor-like activity. *Hum. Mov. Sci.* 26, 275–295.
- Murg, M., Binder, H., and Dimitrijevic, M.R. (2000). Epidural electric stimulation of posterior structures of the human lumbar spinal cord: 1. muscle twitches - a functional method to define the site of stimulation. *Spinal Cord* 38, 394–402.
- North, R., Lanning, A., Hessels, R., and Cutchis, P. (1997). Spinal cord stimulation with percutaneous and plate electrodes: side effects and quantitative comparisons. *Neurosurg. Focus* 2, e3.
- Phillips, L.H., and Park, T.S. (1991). Electrophysiologic mapping of the segmental anatomy of the muscles of the lower extremity. *Muscle Nerve* 14, 1213–1218.
- Pinter, M.M., Gerstenbrand, F., and Dimitrijevic, M.R. (2000). Epidural electrical stimulation of posterior structures of the human lumbosacral cord: 3. Control of spasticity. *Spinal Cord* 38, 524–531.
- Ranger, M.R.B., Irwin, G.J., Bunbury, K.M., and Peutrell, J.M. (2008). Changing body position alters the location of the spinal cord within the vertebral canal: a magnetic resonance imaging study. *Br. J. Anaesth.* 101, 804–809.
- Rattay, F., Minassian, K., and Dimitrijevic, M.R. (2000). Epidural electrical stimulation of posterior structures of the human lumbosacral cord: 2. quantitative analysis by computer modeling. *Spinal Cord* 38, 473–489.
- Richardson, R.R., Cerullo, L.J., McLone, D.G., Gutierrez, F.A., and Lewis, V. (1979). Percutaneous epidural neurostimulation in modulation of paraplegic spasticity. Six case reports. *Acta Neurochir. (Wien)* 49, 235–243.
- Rock, A.K., Truong, H., Park, Y.L., and Pilitsis, J.G. (2019). Spinal cord stimulation. *Neurosurg. Clin. N. Am.* 30, 169–194.
- Schindler-Ivens, S.M., and Shields, R.K. (2004). Soleus H-reflex recruitment is not altered in persons with chronic spinal cord injury. *Arch. Phys. Med. Rehabil.* 85, 840–847.
- Schirmer, C.M., Shils, J.L., Arle, J.E., Cosgrove, G.R., Dempsey, P.K., Tarlov, E., Kim, S., Martin, C.J., Feltz, C., Moul, M., and Magge, S. (2011). Heuristic map of myotomal innervation in humans using direct intraoperative nerve root stimulation. *J. Neurosurg. Spine* 15, 64–70.
- Schoen, N., Chieng, L.O., Madhavan, K., Jermakowicz, W.J., and Vanni, S. (2017). The use of intraoperative electromyogram during spinal cord stimulator placement surgery: a case series. *World Neurosurg.* 100, 74–84.
- Shealy, C.N., Mortimer, J.T., and Reswick, J.B. (1967). Electrical inhibition of pain by stimulation of the dorsal columns: preliminary clinical report. *Anesth. Analg.* 46, 489–491.
- Shils, J.L., and Arle, J.E. (2012). Intraoperative neurophysiologic methods for spinal cord stimulator placement under general anesthesia. *Neuromodulation* 15, 560–572.
- Shils, J.L., and Arle, J.E. (2018). Neuromonitoring for spinal cord stimulation lead placement under general anesthesia. *J. Clin. Neurol.* 14, 444–453.
- Struijk, J.J., Holsheimer, J., and Boom, H.B.K. (1993). Excitation of dorsal root fibers in spinal cord stimulation: a theoretical study. *IEEE Trans. Biomed. Eng.* 40, 632–639.
- Thage, O. (2009). The myotomes L2-S2 in man. *Acta Neurol. Scand.* 41, 241–244.
- Tulgar, M., He, J., Barolat, G., Ketcik, B., Struijk, H., and Holsheimer, J. (1993). Analysis of parameters for epidural spinal cord stimulation. 3. Topographical distribution of paresthesiae—a preliminary analysis of 266 combinations with contacts implanted in the midcervical and midthoracic vertebral levels. *Stereotact. Funct. Neurosurg.* 61, 146–155.
- Wagner, F.B., Mignardot, J.-B., Le Goff-Mignardot, C.G., Demesmaeker, R., Komi, S., Capogrosso, M., Rowald, A., Seáñez, I., Caban, M., Pirondini, E., et al. (2018). Targeted neurotechnology restores walking in humans with spinal cord injury. *Nature* 563, 65–71.
- Wall, E.J., Cohen, M.S., Abitbol, J.J., and Garfin, S.R. (1990). Organization of intrathecal nerve roots at the level of the conus medullaris. *J. Bone Joint Surg. Am.* 72, 1495–1499.
- Whitsel, B., Petrucelli, L., and Sapiro, G. (1969). Modality representation in the lumbar and cervical fasciculus gracilis of squirrel monkeys. *Brain Res.* 15, 67–78.
- York, D.H. (1985). Somatosensory evoked potentials in man: differentiation of spinal pathways responsible for conduction from the forelimb vs hindlimb. *Prog. Neurobiol.* 25, 1–25.

iScience, Volume 24

Supplemental Information

**Spinal motor mapping by epidural
stimulation of lumbosacral
posterior roots in humans**

Ursula S. Hofstoetter, Ivan Perret, Aymeric Bayart, Peter Lackner, Heinrich Binder, Brigitta Freundl, and Karen Minassian

Supplemental Information

Figures S1–S3, Tables S1–S9, Transparent Methods and Supplemental Data

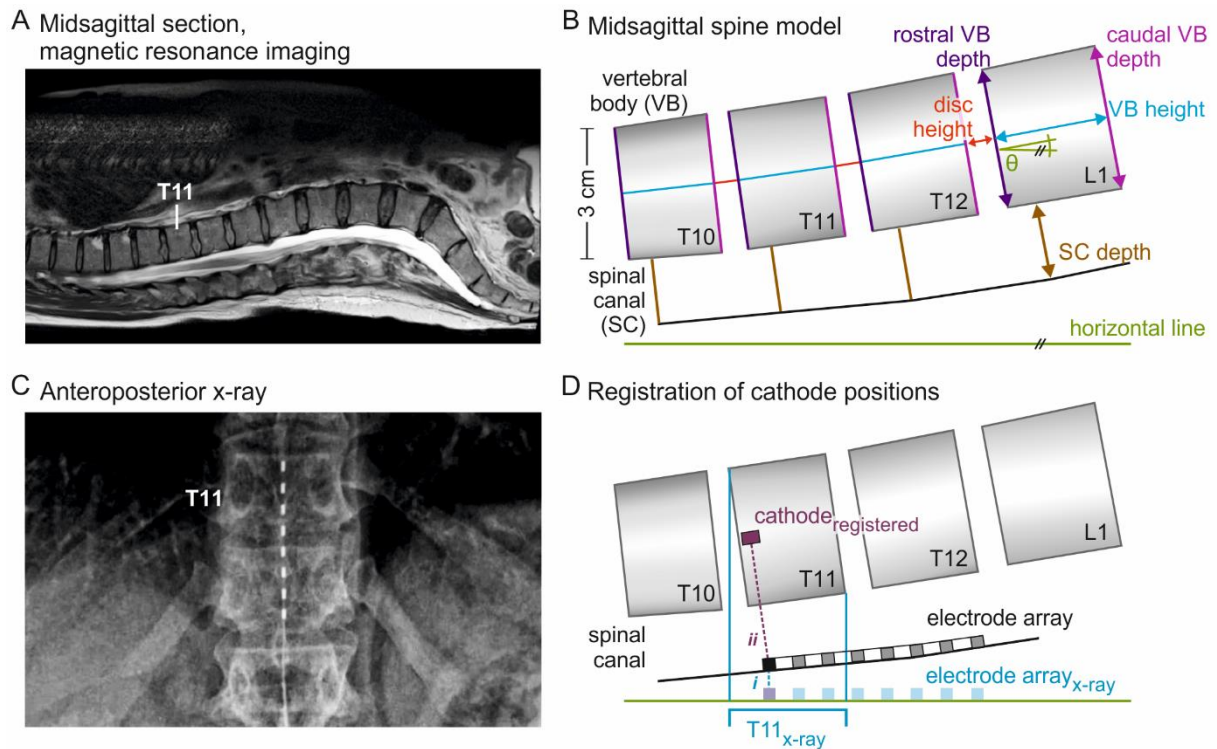


Figure S1. Linking epidural cathode positions to the straight-line spine model; Related to Figure 1. (A) Midsagittal magnetic resonance imaging of the thoracolumbar spine in the supine position shows the curvature of the spinal canal, which is dominated by the thoracic kyphosis in the region of interest. (B) Midsagittal spine model based on vertebral body dimensions, spinal canal depths, and vertebral disc heights as well as inclination angles θ with respect to the horizontal plane. (C) Postoperative anteroposterior x-ray in supine position showing eight midline-located electrodes; subject 32. (D) Transformation of the electrode projection identified from x-ray ($electrode\ array_{x-ray}$) to the midsagittal spine model (line i and electrode array) and position registered into the straight-line model (line ii and $cathode_{registered}$). Sources and values considered in the geometrical spine model are specified in Tables S2 and S3.

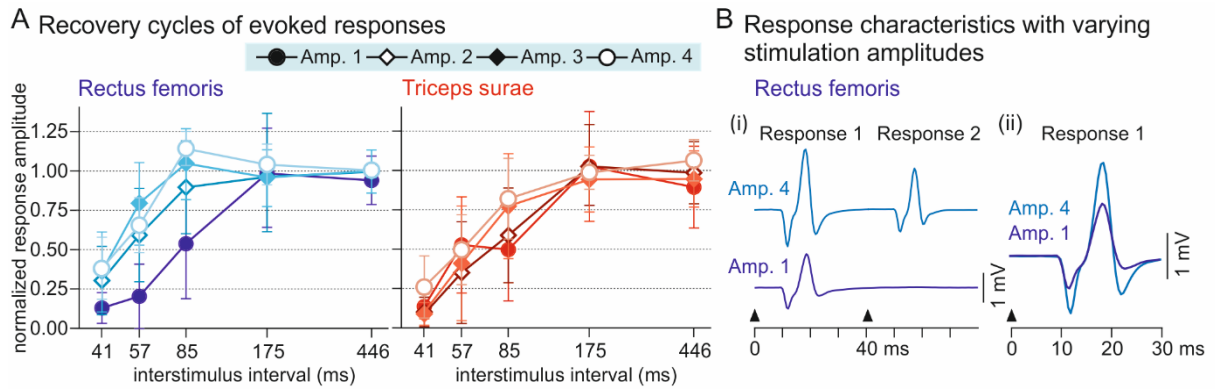


Figure S2. Verification of reflex nature of the epidurally evoked responses; Related to Figure 2.

(A) Recovery cycles of rectus femoris and triceps surae responses (y-axis, mean peak-to-peak amplitudes \pm SE of the second normalized to the first responses) elicited at five different interstimulus intervals as indicated (x-axis, logarithmic scale) and four amplitude (Amp.) categories: Amp. 1, threshold; Amp. 2, (1.0–1.5] x threshold; Amp. 3, (1.5–2.0] x threshold; and Amp. 4, > 2.0 x threshold. Data derived from eight subjects, all with traumatic SCI. (B) (i) Exemplary EMG responses of rectus femoris evoked by double stimuli (arrow heads) with Amp. 1 and Amp. 4, subject 5. (ii) Superimposed representation of the first responses shows unchanged onset latency and EMG shape with increased stimulation amplitude.

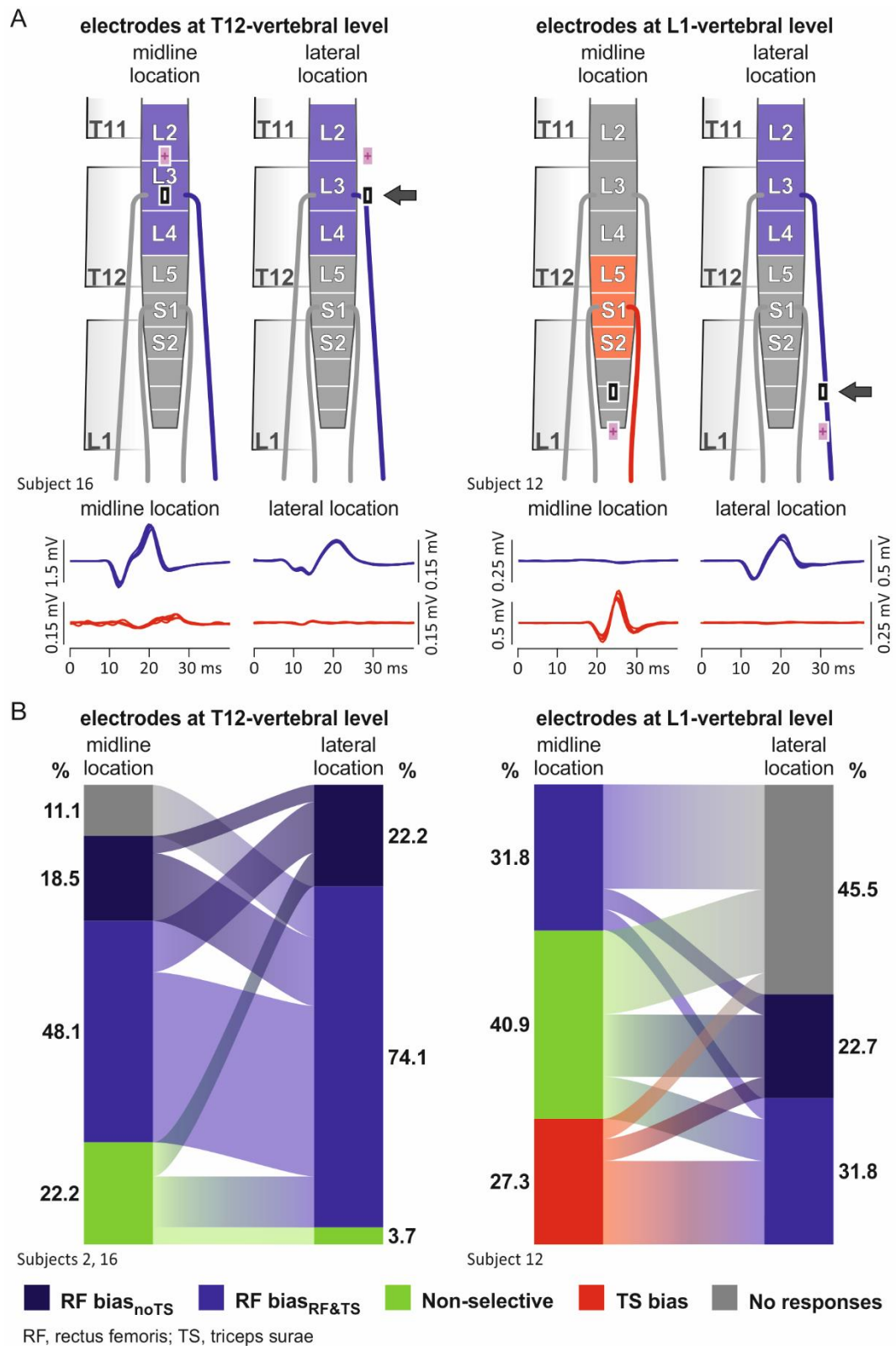


Figure S3. Responses evoked by midline- and laterally located electrodes; Related to Figure 3.

(A) Sketches of midline and lateral electrode locations with respect to spinal cord and root anatomy (posterior view) along with EMG recordings of respectively elicited PRM reflexes evoked in RF and TS at threshold, with cathodes (–; arrows) and anodes (+) at T12- or L1-vertebral levels as indicated; five superimposed responses each. (B) Transitions between RF- and TS-threshold based categories from midline to lateral electrode locations. For electrodes at the T12-vertebral level, 100% of the data sets

obtained with midline-located electrodes that were classified into either of the two RF-bias categories remained within these categories when using laterally located electrodes. Data derived from subjects 2 and 16. For electrodes at the L1-vertebral level, none of the data sets classified into the TS-bias category remained within this category when using laterally placed electrodes, but 66.7% changed to the RF-bias_{RF&T} category and 16.7% each to the RF-bias_{noTS} and the no-responses categories, respectively. Data derived from subject 12.

Table S1. Clinical characteristics of subject population; Related to Figures 1–6.

Subject No.	Gender	Age* (y)	Diagnosis	AIS Grade	Neurological level of injury	SCI chronicity* (y)
1	m	26.7	SCI	A	C4	1.8
2	m	18.0	SCI	A	C4	2.9
3	m	25.6	SCI	A	C4	3.8
4	m	36.6	SCI	A	C7	4.6
5	m	21.9	SCI	A	C7	5.1
6	m	50.6	SCI	A	T3	1.6
7	f	18.0	SCI	A	T5	1.2
8	f	30.9	SCI	A	T5	1.4
9	f	32.8	SCI	A	T5	2.5
10	m	27.2	SCI	A	T6	7.6
11	m	24.5	SCI	A	T7	1.1
12	m	21.3	SCI	A	T7	2.6
13	f	24.7	SCI	A	T7	4.2
14	m	29.5	SCI	A	T7	7.9
15	m	33.2	SCI	A	T8	13.5
16	m	29.0	SCI	B	C6	2.5
17	m	28.0	SCI	B	C6	8.1
18	m	25.3	SCI	B	C8	1.6
19	f	22.6	SCI	B	T2	5.9
20	m	57.7	SCI	B	T9	2.5
21	m	31.8	SCI	C	C3	6.3
22	m	22.0	SCI	C	C7	6
23	m	56.4	SCI	C	C8	2.1
24	f	21.9	SCI	C	T6	1.2
25	m	53.3	SCI	D	C7	2.7
26	m	61.8	SCI	D	T4	43.3
27	m	57.0	HSP	NA	NA	NA
28	m	53.2	HSP	NA	NA	NA
29	f	57.9	PH	NA	NA	NA
30	m	50.2	MS	NA	NA	NA
31	f	55.7	MS	NA	NA	NA
32	m	40.3	MS	NA	NA	NA
33	m	49.8	MS	NA	NA	NA

*at time of epidural electrode implantation; AIS, American Spinal Injury Association impairment scale; HSP, hereditary spastic paralysis; MS, multiple sclerosis; PH, perinatal hypoxia; SCI, traumatic spinal cord injury; TBI, traumatic brain injury. The Expanded Disability Status Scale scores of the MS patients ranged from 5–7.5. The individual with TBI was implanted 2.5 years after trauma.

Table S2. Sources considered in the geometrical spine model; Related to Figure 1.

T10–L1 vertebral body and intervertebral disc heights	Vertebral levels studied	Applied weight
Koeller et al., Spine 1984, 9: 725–733	T5–L5 (intervertebral disc heights)	2
Nissan et al., Eng Med 1984, 13: 111–114	C2–C7, L1–L5 (vertebral body and intervertebral disc heights)	3
Berry et al., Spine 1987, 12: 362–367	T2, T7, T12, L1–L5 (vertebral body heights)	2
Scoles et al., Spine 1988, 13:1082–1086	T1, T3, T6, T9, T12, L1, L3, L5 (vertebral body heights)	2
Panjabi et al., Spine 1991, 16: 888–901	T1–T12 (vertebral body heights)	2
Panjabi et al., Spine 1992, 17: 299–306	L1–L5 (vertebral body heights)	2
Fang et al., J Spinal Disord 1994, 7: 307–316	L1–L5 (intervertebral disc heights)	3
Tan et al., Eur Spine J 2004, 13: 137–146	C3–L5 (vertebral body heights)	1
Busscher et al., Eur Spine J 2010, 19: 1104–1114	C3–L5 (vertebral body and intervertebral disc heights)	1
Kunkel et al., J Anat 2011, 219: 375–387	C7–T12 (vertebral body and intervertebral disc heights)	2
Singh et al., Asian Spine J 2011, 5: 20–34	T1–T12 (vertebral body heights)	3
Fletcher et al., Eur Spine J 2015, 24: 2321–2329	T2, T4, T6, T8, T10 (intervertebral disc heights)	3
Demir et al., Anatomy 2018, 12: 34–37	T12–L5 (intervertebral disc heights)	3
Frost et al., Materials 2019, 12: E253	C2–L5 (intervertebral disc heights)	4
Anteroposterior dimensions of T10–L1 vertebral bodies	Vertebral levels studied	Applied weight
Nissan et al., Eng Med 1984, 13: 111–114	C2–C7, L1–L5	3
Berry et al., Spine 1987, 12: 362–367	T2, T7, T12, L1–L5	2
Krag et al., Spine 1988, 13: 27–32	T9–L5	2
Scoles et al., Spine 1988, 13:1082–1086	T1, T3, T6, T9, T12, L1, L3, L5	2
Panjabi et al., Spine 1991, 16: 888–901	T1–T12	2
Panjabi et al., Spine 1992, 17: 299–306	L1–L5	2
Fang et al., J Spinal Disord 1994, 7: 307–316	L1–L5	3
Laporte et al. Eur J Orthop Surg Traumatol 2000, 10: 85–91	T1–T12	2
Tan et al., Eur Spine J 2004, 13: 137–146	C3–L5	1
Spinal canal depth	Vertebral levels studied	Applied weight
Cotterill et al., J Orthop Res 1986, 4: 298–303	T6, T2, L3	1
Berry et al., Spine 1987, 12: 362–367	T2, T7, T12, L1–L5	2
Scoles et al., Spine 1988, 13:1082–1086	T1, T3, T6, T9, T12, L1, L3, L5	2
Panjabi et al., Spine 1991, 16: 888–901	T1–T12	2
Panjabi et al., Spine 1992, 17: 299–306	L1–L5	2
Holsheimer et al., Am J Neuroradiol 1994, 15: 951–959	C4–C6, T5, T6, T11, T12	2
Laporte et al. Eur J Orthop Surg Traumatol 2000, 10: 85–91	T1–T12	2
Tan et al., Eur Spine J 2004, 13: 137–146	C3–L5	1
Inclination angles of T10–L1 vertebral bodies and intervertebral discs	Number of MRIs considered	
Huk W, Gademann G, Friedmann G. Magnetic resonance imaging of central nervous system diseases: functional anatomy - imaging, neurological symptoms - pathology. Springer; 1990	2	
Schnitzlein HN, Murtagh FR. Imaging anatomy of the head and spine: a photographic color atlas of MRI, CT, gross,	3	

and microscopic anatomy axial, coronal, and sagittal planes. 2nd ed. Baltimore: Urban & Schwarzenberg; 1990	
Pomeranz SJ. MRI total body atlas: 1: Neuro. Cincinnati, Ohio: MRI-EFI - Publ.; 1992	1
Ellis H, Logan B, Dixon A. Human sectional anatomy. 2nd ed. Butterworth-Heinemann; 1999	1
Küper K. MR/CT-Atlas der Anatomie. Georg Thieme Verlag; 2001	5
Uhlenbrock D. MRT der Wirbelsäule und des Spinalkanals. Stuttgart: Thieme; 2001	4
Weyreuther M, Heyde CE, Westphal M, Zierski J, Weber U. MRI Atlas: Orthopedics and Neurosurgery: The Spine. Berlin, Heidelberg: Springer Berlin Heidelberg New York; 2007	7
Forseen S, Borden N. Imaging Anatomy of the Human Spine. Springer Publishing Company; 2015	7
Ross JS, Moore KR. Spine. 3rd ed. Philadelphia, Pennsylvania: Elsevier Amirsys; 2015	3
mrmaster.com (https://mrmaster.com/anatomy%20spine%20L%20spine%20sagittal.html , accessed: 2020/01/16)	1

Table S3. Values considered in the geometrical spine model; Related to Figure 1.

Vertebral body	Vertebral body height (weighted mean, mm)	Intervertebral disc height (weighted mean, mm)	Anteroposterior dimension (weighted mean, mm)		Spinal canal depth (weighted mean, mm)	Inclination angle (degree)
			<i>Rostral</i>	<i>Caudal</i>		
T10	20.497		29.160	30.830	14.660	6.341
T10-T11		5.417				7.267
T11	21.578		30.640	30.796	14.829	8.193
T11-T12		5.716				9.045
T12	23.512		30.800	31.656	16.458	9.897
T12-L1		6.589				10.281
L1	25.372		30.912	32.075	17.171	10.666

Table S4. Sources considered in the spinal cord model; Related to Figure 1.

Segmental heights of lumbosacral spinal cord	Spinal cord segments studied	Applied weight
Donaldson & Davis, J Comp Neurol 1903, 13: 19–40	C1–S5	1
Sharrard, Ann R Coll Surg Engl 1964, 35:106–122	T12–S5	1
Yamada et al., J Neurosurg 1976, 45: 683–691	T12–S5	2
d’Avella & Mingrino, J Neurosurg 1979, 51: 819–823	L1–S5	2
Lang, 1984, In: Hohmann, Kügelgen, Liebig, Schirmer, eds. ISBN: 978-3-642-68975-8, Berlin: Springer	T12–S5	2
Mersdorf et al., J Urol 1993, 149: 345–349	S1–S5	1
Ko H-Y et al., Spinal Cord 2004, 42: 35–40	C3–S5	2
Hauck et al., J Neurosurg Spine 2008, 9: 207–212	S1–S5	2
Termination levels of conus medullaris		Applied weight
Saifuddin et al., Spine 1998; 23: 1452–1456		4
Demiryürek et al., Clin Imaging 2002, 26: 375–377		4
Kim et al., Anesthesiology 2003, 99: 1359–1363		4
Sevinc et al., Neuroradiol J 2006, 19: 375–378		3
Moussallem et al., Anat Res Int. 2014, 2014: 1–4		2
Rostamzadeh et al., Int J Epidemiol Res 2015, 2: 118–125		3
Karabulut et al., Int J Morphol 2016, 34: 1352–135		4
Kwon et al., Korean J Phys Anthropol 2016, 29: 47		3
Nasr, Folia Morphol 2016, 75: 287–299		3
Preeti & Chaturvedi, Int J Sci Res 2016, ISSN Online 14: 2319–7064		1
Liu et al., Surg Radiol Anat 2017, 39: 759–765		4
Moon et al., Asian Spine J 2019, 13: 313–317		2

Table S5. Values considered in the spinal cord model; Related to Figure 1.

Spinal cord segment	Segmental height (weighted mean, mm)
L1	12.627
L2	11.213
L3	9.803
L4	8.786
L5	7.369
S1	6.664
S2	6.265
S3	5.412
S4	4.587
S5	3.595

Table S6. Termination levels of the conus medullaris derived from literature; Related to Figure 1.

Termination levels – Bin	Normalized occurrence counts (weighted mean)
T11, lower third	0.0002
T11–T12 intervertebral disc	0.0009
T12, upper third	0.0026
T12, middle third	0.0091
T12, lower third	0.0274
T12–L1 intervertebral disc	0.0968
L1, upper third	0.1312
L1, middle third	0.1571
L1, lower third	0.1987
L1–L2 intervertebral disc	0.1855
L2, upper third	0.0881
L2, middle third	0.0496
L2, lower third	0.0232
L2–L3 intervertebral disc	0.0120
L3, upper third	0.0051
L3, middle third	0.0056
L3, lower third	0.0046
L3–L4 intervertebral disc	0.0021
L4, upper third	0.0000
L4, middle third	0.0002

Table S7. PRM-reflex recruitment in subjects with traumatic SCI vs. non-SCI subjects; Related to Figure 3.

	EES amp. (V)	EMG response amplitudes				
		Add amp. (μ V)	RF amp. (μ V)	TA amp. (μ V)	Ham amp. (μ V)	TS amp. (μ V)
RF-bias category, threshold						
SCI	4.7 \pm 0.3	364.1 \pm 43.7	373.7 \pm 61.6	NA	329.6 \pm 61.4	NA
Non-SCI	5.0 \pm 0.6	454.3 \pm 64.0	252.2 \pm 108.8	NA	465.2 \pm 108.7	NA
Results of LMM	F(1,18.913) = .203, P = .657, η_p^2 = .011	F(1,16.288) = 1.355, P = .261, η_p^2 = .077	F(1,20.914) = .946, P = .342, η_p^2 = .043	NA	F(1,22.629) = 1.180, P = .289, η_p^2 = .050	NA
RF-bias category, common threshold						
SCI	5.8 \pm 0.4	1150.2 \pm 139.9	1354.1 \pm 195.6	101.3 \pm 13.1	1246.8 \pm 145.2	202.8 \pm 39.9
Non-SCI	6.2 \pm 0.7	849.8 \pm 200.9	711.6 \pm 341.9	77.8 \pm 22.6	795.7 \pm 254.2	178.6 \pm 70.0
Results of LMM	F(1,18.715) = .376, P = .547, η_p^2 = .020	F(1,15.451) = 1.507, P = .238, η_p^2 = .089	F(1,22.117) = 2.661, P = .117, η_p^2 = .107	F(1,20.288) = .808, P = .379, η_p^2 = .039	F(1,21.776) = 2.375, P = .138, η_p^2 = .098	F(1,20.380) = .091, P = .766, η_p^2 = .004
RF-bias category, maximum stimulation						
SCI	8.5 \pm 0.5	1300.2 \pm 145.7	1543.3 \pm 226.0	357.5 \pm 65.7	1579.6 \pm 163.2	743.7 \pm 141.6
Non-SCI	7.4 \pm 0.9	941.9 \pm 215.1	820.7 \pm 401.5	249.4 \pm 116.6	889.4 \pm 289.7	412.0 \pm 251.3
Results of LMM	F(1,19.823) = 1.160, P = .294, η_p^2 = .055	F(1,16.766) = 1.902, P = .186, η_p^2 = .102	F(1,21.881) = 2.459, P = .131, η_p^2 = .101	F(1,20.052) = .654, P = 428, η_p^2 = .032	F(1,22.799) = 4.310, P = .049, η_p^2 = .159	F(1,19.574) = 1.322, P = .264, η_p^2 = .063

Add, adductors; Amp., amplitude; EES, epidural electrical stimulation; Ham, hamstrings muscle group; LMM, linear mixed model; Non-SCI, subjects with an upper motoneuron disorder other than traumatic spinal cord injury, N = 6 included in this analysis; PRM reflex, posterior root-muscle reflex; RF, rectus femoris; SCI, subjects with traumatic spinal cord injury, N = 19. TA, tibialis anterior; TS, triceps surae muscle group.

Table S8. PRM-reflex recruitment in subjects with motor-complete SCI vs. subjects with motor-incomplete SCI; Related to Figure 3.

	EES amp. (V)	Add amp. (μ V)	EMG response amplitudes			
			RF amp. (μ V)	TA amp. (μ V)	Ham amp. (μ V)	TS amp. (μ V)
RF-bias category, threshold						
Motor-complete	4.8 \pm 0.4	356.0 \pm 69.0	412.1 \pm 84.1	NA	363.3 \pm 79.7	NA
Motor-incomplete	4.5 \pm 0.7	371.1 \pm 72.3	295.0 \pm 120.1	NA	258.5 \pm 114.1	NA
Results of LMM	F(1,14.999) = .147, P = .707, η_p^2 = .010	F(1,11.264) = .023, P = .882, η_p^2 = .002	F(1,15.563) = .637, P = .437, η_p^2 = .039	NA	F(1,17.203) = .566, P = .462, η_p^2 = .032	NA
RF-bias category, common threshold						
Motor-complete	6.0 \pm 0.4	1240.5 \pm 224.9	1438.8 \pm 263.4	99.9 \pm 15.5	1398.0 \pm 182.3	202.0 \pm 54.5
Motor-incomplete	5.2 \pm 0.7	1032.9 \pm 259.4	1144.5 \pm 417.1	104.4 \pm 23.8	892.9 \pm 286.7	204.3 \pm 85.3
Results of LMM	F(1,16.007) = 1.268, P = .277, η_p^2 = .073	F(1,9.308) = .366, P = .560, η_p^2 = .038	F(1,15.446) = .356, P = .559, η_p^2 = .023	F(1,16.319) = .025, P = .876, η_p^2 = .002	F(1,14.714) = 2.210, P = .158, η_p^2 = .131	F(1,15.923) < .001, P = .983, η_p^2 < .001
RF-bias category, maximum stimulation						
Motor-complete	8.7 \pm 0.6	1486.2 \pm 233.2	1723.7 \pm 306.4	451.6 \pm 72.0	1858.2 \pm 195.1	938.0 \pm 181.1
Motor-incomplete	7.2 \pm 0.9	1096.3 \pm 247.8	1161.7 \pm 446.0	154.2 \pm 103.6	1023.9 \pm 280.8	335.1 \pm 260.9
Results of LMM	F(1,16.897) = 1.996, P = .176, η_p^2 = .106	F(1,10.614) = 1.314, P = .277, η_p^2 = .110	F(1,15.937) = 1.079, P = .315, η_p^2 = .063	F(1,13.906) = 5.557, P = .034, η_p^2 = .286	F(1,15.661) = 5.954, P = .027, η_p^2 = .275	F(1,14.264) = 3.604, P = .078, η_p^2 = .202

Add, adductors; Amp., amplitude; EES, epidural electrical stimulation; Ham, hamstrings muscle group; LMM, linear mixed model; Motor-complete, subjects with motor-complete traumatic spinal cord injury, AIS grades A or B, N = 13 included in this analysis; Motor-incomplete, subjects with motor-incomplete traumatic spinal cord injury, AIS grades C or D, N = 6; PRM reflex, posterior root-muscle reflex; RF, rectus femoris; TA, tibialis anterior; TS, triceps surae muscle group

Table S9. Transitions between RF- and TS-threshold based categories from midline- to laterally located electrodes; Related to Figure S3.

Electrodes at T12-vertebral level

Midline cathode	Lateral cathode				
	No responses	RF bias _{noTS}	RF bias _{RF&TS}	Non-selective	TS bias
No responses	0.0%	11.1%	0.0%	0.0%	0.0%
RF bias _{noTS}	0.0%	3.7%	14.8%	0.0%	0.0%
RF bias _{RF&TS}	0.0%	11.1%	37.0%	0.0%	0.0%
Non-selective	0.0%	7.4%	11.1%	3.7%	0.0%
TS bias	0.0%	0.0%	0.0%	0.0%	0.0%

Electrodes at L1-vertebral level

Midline cathode	Lateral cathode				
	No responses	RF bias _{noTS}	RF bias _{RF&TS}	Non-selective	TS bias
No responses	0.0%	0.0%	0.0%	0.0%	0.0%
RF bias _{noTS}	0.0%	0.0%	0.0%	0.0%	0.0%
RF bias _{RF&TS}	22.7%	4.5%	4.5%	0.0%	0.0%
Non-selective	18.2%	13.6%	9.1%	0.0%	0.0%
TS bias	4.5%	4.5%	18.2%	0.0%	0.0%

Transparent Methods

Human subjects

Data were derived from 34 individuals who had been referred to a clinical program for the treatment of lower-extremity spasticity by epidural electrical stimulation of the spinal cord (EES) (Pinter et al., 2000). The sample included 26 individuals with chronic traumatic SCI (median time post-injury: 2.7 years, IQR: 1.6–5.7), two with hereditary spastic paralysis, one with perinatal hypoxia, four with multiple sclerosis, and one with traumatic brain injury (Table S1). Supine anteroposterior x-rays of the thoracolumbar spine obtained after the surgical implantation of the epidural lead as well as EMG data of lower-extremity muscle responses evoked by midline-located epidural linear leads in the supine position were available from all subjects. Subjects 2, 12, and 16 were tested with additional, bilaterally placed percutaneous linear leads during the trial phase, with the electrodes of both leads positioned at the rostrocaudal levels of the midline ones. In 16 subjects of the 34 with postoperative recordings, EMG data were also available from intraoperative neurophysiological monitoring. Retrospective data analysis was approved by the Ethics Committee of the City of Vienna (EK-17-239-VK, EK-17-059-VK).

Postoperative stimulation and recordings

Postoperative EMG recordings were obtained either during the trial phase ($n = 18$), with the epidural lead externalized and connected to a test stimulator, or after full implantation of the epidural system ($n = 16$), with the lead connected to an implantable pulse generator. Epidural lead models were 3487A Pisces Quad (array length 30 mm; $n = 20$), 3877 Octad Standard (66 mm; $n = 6$), and Vectris® SureScan® MRI Model 977A2 1x8 Compact (52 mm; $n = 8$), all by Medtronic (Minneapolis, MN). The leads carried either four (3487A) or eight (3877, 977A2) cylindrical electrodes, each with a diameter of 1.3 mm and a length of 3 mm. Inter-electrode spacing was 6 mm (3487A, 3877) or 4 mm (977A2). Test stimulator models were 3625-G ($n = 5$), 37022 ($n = 10$), and 97725 ($n = 3$), and implantable pulse generator models were Itrel 3 ($n = 15$) and PrimeAdvanced SureScan MRI ($n = 1$). Pulse width was set at 280 μ s in subjects 6 and 26, and at 210 μ s in all other subjects. Bipolar electrode combinations with different spacing between the active electrodes and with the anode either rostral or caudal to the cathode were tested. Monopolar stimulation was carried out by setting one electrode as cathode and the implantable pulse generator case as anode. With a given electrode setup, stimulation was applied at the lowest programmable frequency (test stimulators: 2 Hz, $n = 10$; 2.5 Hz, $n = 3$; 6.5 Hz, $n = 5$; implantable pulse generators: 2 Hz, $n = 1$; 2.2 Hz, $n = 15$). Stimulation amplitude was increased in increments of 0.5 or 1 V (or mA, $n = 3$) up to a maximum of 10 V (10 mA) or below if responses had plateaued or stimulation started to cause discomfort. For each amplitude, stimulation was applied for 15–30 s.

All postoperative EMG recordings were conducted in the supine position. Pairs of silver-silver chloride surface EMG electrodes (Intec Medizintechnik GmbH, Klagenfurt, Austria) were placed with an inter-electrode distance of 3 cm bilaterally over RF, Ham, TA, and TS (Hofstoetter et al., 2018). EMG data from Add were additionally acquired in 25 subjects. A common ground electrode was placed over the iliac crest. Abrasive paste (Nuprep, Weaver and Company, Aurora, CO) was used for skin preparation to reduce EMG electrode resistance below 5 k Ω . EMG electrodes placed over the lower rectus abdominis and paraspinal muscles captured stimulation artifacts used to identify the onsets of

stimulation pulses. EMG signals were amplified (Grass Instruments, Quincy, MA) with a gain of 2000, filtered to a bandwidth of 30–700 Hz, and digitized at 2002 samples per second and channel using a Coda ADC system (Dataq Instruments, Akron, OH) in 20 subjects. In the remaining subjects, the Phoenix multi-channel EMG system (EMS-Handels GmbH, Korneuburg, Austria) was used, set to a gain of 502 over a bandwidth of 10–1000 Hz and digitized at 2048 samples per second and channel.

Intraoperative stimulation and recordings

Intraoperative recordings were derived while patients were in the prone position. The lead was connected to an external test stimulator (3625-G, n = 2; 37022, n = 11; 97725, n = 3), which delivered stimulation at 2 Hz, n = 11; 2.5 Hz, n = 3; and 6.5 Hz, n = 2. Stimulation amplitude was increased in increments of 0.5 or 1 V (or mA, n = 3). Surface EMG electrode model, skin preparation and EMG locations were same as for the postoperative recordings. Evoked responses were recorded using a Phoenix EMG system, set to a gain of 4664 over a bandwidth of 10–500 Hz and digitized at 1024 samples per second and channel. EMG recordings obtained with the final position of the epidural lead were analyzed for the current study. No muscle relaxants were used during the intraoperative monitoring. The surgical technique was minimally invasive and performed awake, with the percutaneous lead inserted into the epidural space through a Tuohy needle under local anesthesia.

Geometrical model of the spine and the lumbosacral spinal cord

Imaging techniques depict electrode positions of an epidural array with respect to vertebral levels, but cannot identify specific spinal cord segments. We thus created a statistically sound anatomical model to interface vertebral electrode sites with spinal cord segmental positions and to link the evoked responses to the segmental organization of the lumbosacral spinal cord.

We constructed a straight-line model of the spine composed of weighted mean values of vertebral body heights (Berry et al., 1987; Busscher et al., 2010; Kunkel et al., 2011; Nissan and Gilad, 1984; Panjabi et al., 1992, 1991; Scoles et al., 1988; Singh et al., 2011; Tan et al., 2004) and intervertebral disc heights of T10–L1 (Busscher et al., 2010; Demir et al., 2018; Fang et al., 1994; Fletcher et al., 2015; Frost et al., 2019; Koeller et al., 1984; Kunkel et al., 2011; Nissan and Gilad, 1984). Weights applied on the mean values reflected the sample sizes of the respective sources, yet avoided a bias introduced by single studies with very large sample sizes. We defined: 1 for studies with N = 1–10 subjects, 2 for N = 11–99, 3 for N = 100–199, and 4 for N > 199. The weighted mean values used for our anatomical model were calculated as:

$$\bar{x} = \frac{\sum_{i=1}^m w_i \cdot x_i}{\sum_{i=1}^m w_i}$$

with w_i the weight and x_i the mean value of the i^{th} study, and m , the total number of studies considered. References and values, Tables S2 and S3.

We integrated a straight-line geometrical model of the lumbosacral spinal cord into the spine model, built bottom-up using the vertebral level of termination of the conus medullaris as a starting point.

This point was defined considering twelve in-vivo magnetic resonance imaging studies that reported the occurrence count of the termination level in relation to the upper, middle, or lower third of the respective vertebral body or to the respective intervertebral disc (bins), with a total of 4797 subjects (Demiryürek et al., 2002; Karabulut et al., 2016; Kim et al., 2003; Kwon et al., 2016; Liu et al., 2017; Moon et al., 2019; Moussallem et al., 2014; Nasr, 2016; Preeti and Chaturvedi, 2016; Rostamzadeh et al., 2015; Saifuddin et al., 1998; Sevinc et al., 2006). We constructed a distribution of occurrence counts from the data set of each study by normalizing the occurrence counts per bin to the total number of counts. The final distribution was obtained by weighted averaging of these distributions. Weights were: 1 for studies with $N = 1-99$ subjects, 2 for $N = 100-199$, 3 for $N = 200-499$, and 4 for $N > 499$. We used the median of this skewed distribution as the termination level in our model. For the calculation of the margin of error e for our sample of 34 subjects, given a 95% confidence level, we assumed a normal population distribution and considered the median as the mean value. The population standard deviation was estimated from the 14th to the 81st percentiles (thereby overestimating the dispersion of the population distribution), and corresponded to $\sigma = \pm 16.89$ mm in our anatomical model. The margin of error e was ± 5.68 mm with respect to the population median, derived from the formula for calculating sample sizes:

$$N = \frac{z^2 \cdot \sigma^2}{e^2}$$

with $N = 34$, $z = 1.96$ (critical value for the chosen confidence interval).

To construct the straight-line spinal cord model, we used mean values of spinal cord segmental heights of S5–L1 from eight anatomical studies (d'Avella and Mingrino, 1979; Donaldson and Davis, 1903; Hauck et al., 2008; Ko et al., 2004; Lang, 1984; Mersdorf et al., 1993; Sharrard, 1964; Yamada et al., 1976). Weighted mean values were calculated using the same method as for the construction of the spine model. We stacked weighted mean heights of the segments one by one from the S5 to the L1 segment, starting from the conus medullaris termination level. References and values, Tables S4–S6.

Segmental innervations of lower-extremity muscles

To obtain a spatial relation between rostrocaudal cathode sites and expected segmental distributions of motoneuron pools that innervate lower-extremity muscles, we constructed a probability map of lower-extremity muscle innervation, which integrated qualitative data from textbooks of anatomy (Bing, 1948; Cunningham, 1991; DeJong, 1979; Foerster and Bumke, 1936; Gray, 1989; Haymaker and Woodhall, 1953; Spalteholz, 1923) and quantitative data from electrophysiological studies (Liguori et al., 1992; Phillips and Park, 1991; Schirmer et al., 2011; Sharrard, 1964; Thage, 2009). The textbooks reported the importance of innervation qualitatively or illustrated the segmental innervations in charts. We assigned values of 0%, 20%, 25%, 33.3%, 50%, 66.7%, and 100% to each spinal segment according to its qualitatively described contribution to muscle innervation. The electrophysiological studies reported the muscles responding to stimulation of specific spinal roots. We related the number of times a muscle was activated to the total number of times a segment was stimulated. We obtained values of 0–100% by normalizing the innervation probability of each segment supplying a muscle to that of the key segment. We combined innervation probabilities derived from the textbooks and the electrophysiological studies and used mean values for our model.

Registration of cathode positions into the spine model

We derived the rostrocaudal cathode positions from postoperative anteroposterior x-rays in supine position. Cathode positions in our spine model had to be deduced from the anteroposterior x-ray projections of electrode arrays that were tilted in the midsagittal plane because of the spinal curvature (Figure S1A). We constructed a midsagittal cross-sectional spine model (Figure S1B) using anteroposterior dimensions of the vertebral bodies measured at the upper and lower end-plates (Berry et al., 1987; Fang et al., 1994; Krag et al., 1988; Laporte et al., 2000; Nissan and Gilad, 1984; Panjabi et al., 1992, 1991; Scoles et al., 1988; Tan et al., 2004) and the spinal canal anteroposterior diameter (Berry et al., 1987; Cotterill et al., 1986; Holsheimer et al., 1994; Laporte et al., 2000; Panjabi et al., 1992, 1991; Scoles et al., 1988; Tan et al., 2004). Vertebral body and intervertebral disc heights as well as weights were same as in the straight-line spine model. The spinal curvature in the midsagittal plane was created by rotating the vertebral bodies by their inclination angles θ with respect to the horizontal plane (Figure S1B). Inclination angles of the vertebral bodies T10–L1 in our model were calculated as the mean value of the angles of the dorsal and ventral vertebral body border derived from midsagittal magnetic resonance images (34 subjects) of the thoracolumbar spine (Gybels J, Van Roost D, 1985; Huk et al., 1990; Schnitzlein and Murtagh, 1990; Pomeranz, 1992; Ellis et al., 1999; Küper, 2001; Uhlenbrock, 2001; Weyreuther et al., 2007; Forseen and Borden, 2015; mrimaster.com). To model the spinal canal, one key point per vertebral body was obtained by adding weighted means of the spinal canal depth derived from literature at 75% of the vertebral body height. The posterior border of the spinal canal was drawn as linear interpolation between these points. References and values, Tables S2 and S3.

We identified the electrode positions with respect to the most rostral and caudal borders of the vertebral body projections in the x-rays (Figure S1C) and entered these relative positions into the midsagittal spine model as horizontal projections (Figure S1D, electrode array_{x-ray}). The intersection of a vertical line drawn from the projection of an electrode (dashed line *i* in Figure S1D) with the posterior border of the spinal canal defined the “actual” position of the electrode in the epidural space of the model (Figure S1D, electrode array). A line drawn from this electrode position perpendicular to the midline of the vertebral body (dashed line *ii* in Figure S1D) gave the longitudinal position of the electrode in the straight-line spine model (Figure S1D, cathode_{registered}). We computerized the graphical transformation from the projected electrode sites to the straight-line spine model by analytically implementing the cross-sectional model (Matlab R2019a, The MathWorks, Inc., Natick, MA, USA). The transformation followed the same steps as described above graphically, with segment-wise-defined functions corresponding to the anatomical elements. The positions of electrodes used as cathode in the available data were registered as longitudinal coordinates (mm) in the straight-line spine model, with 0 mm at the lower end-plate of the L1-vertebral body.

Demonstration of reflex nature of evoked responses

We had previously demonstrated the reflex nature of responses evoked by mid-line placed cylindrical electrodes as used here (Hofstoetter et al., 2018; Minassian et al., 2016, 2004). To affirm that, across stimulation sites and amplitudes, EES would map the segmental anatomy of the lumbosacral

spinal cord through the electrical stimulation of proprioceptive afferents also in the present study, we investigated whether RF and TS responses would demonstrate post-stimulation depression when tested by paired pulses, a hallmark characteristic of monosynaptic reflexes (Hofstoetter et al., 2019; Magladery et al., 1951; Pierrot-Deseilligny and Burke, 2012). To this end, we analyzed data from a subpopulation of the subjects (N = 8; all with traumatic SCI) in whom an additional protocol was conducted to study the effects of stimulation frequency. For a given electrode setup, stimulation was applied at increasing frequencies and with incremental intensities of up to 10 V. We extracted EMG responses evoked by the first two stimuli of the trains with interstimulus intervals of 41 ms, 57 ms, 85 ms, 175 ms, and 446 ms. We also considered the effect of stimulation amplitude (four amplitude categories: threshold; (1.0–1.5] x threshold; (1.5–2.0] x threshold; and > 2.0 x threshold) to exclude that stronger stimulation would directly activate alpha-motoneuron axons within the anterior roots due to current spread in the cerebrospinal fluid (Capogrosso et al., 2013). EMG peak-to-peak amplitudes of the second responses were normalized to those of the first responses. Mean normalized peak-to-peak amplitudes were calculated for each interstimulus interval, and separate recovery cycles for RF and TS responses were obtained per stimulation-amplitude category. To investigate the effect of stimulation amplitude and interstimulus interval (repeated measures), separate mixed analyses of variance (ANOVAs) were run.

The onset latencies of the RF responses evoked by the first stimulus of the pair with an interstimulus interval of 41 ms for the four different amplitude categories were analyzed. Response onset was defined as the first deflection of the EMG potential from baseline that exceeded 5% of the peak-to-peak amplitude of the response. Median onset latencies were calculated for each amplitude category and compared using a Kruskal-Wallis test.

Mapping of the lumbosacral spinal cord by means of relative response thresholds

We investigated whether threshold stimulation would reflect the segmental cathode site. To this end, we classified the rostrocaudal cathode distribution and the associated evoked responses from postoperative EMG recordings (stimulation frequencies 2–6.5 Hz) of the 34 subjects into four categories according to the relative RF and TS thresholds (Th). Threshold was defined as the lowest stimulation amplitude that evoked average peak-to-peak amplitudes $\geq 50 \mu\text{V}$ across the available responses. The categories were: no responses evoked in RF and TS with stimulation up to the maximum (10 V or 10 mA); responses evoked with $\text{Th}_{\text{RF}} < \text{Th}_{\text{TS}}$ (RF bias); non-selective stimulation with $\text{Th}_{\text{RF}} = \text{Th}_{\text{TS}}$; and responses evoked with $\text{Th}_{\text{RF}} > \text{Th}_{\text{TS}}$ (TS bias). Data derived from the two legs of a subject with the same stimulation settings could fall into two different categories and were considered separately. A total of 570 data sets, considering 34 subjects, two legs, and the number of individually tested mono- and bipolar electrode setups, were analyzed. Eleven subjects contributed 4–10 data sets, twelve contributed 11–20, five contributed 21–30, and another six contributed 31–40 data sets. EMG responses of 72 data sets were evoked by monopolar stimulation, and of 498 data sets by bipolar stimulation. The cathode distributions (registered coordinates in the spine model) of the four categories were compared using a Kruskal-Wallis test. The thresholds of RF and TS responses, respectively, were compared between categories using separate Kruskal-Wallis tests. Within the RF-bias and the TS-bias categories (considering only data sets with both RF and TS responding), the thresholds of RF and TS were compared using Wilcoxon signed-rank tests. Additionally, the response thresholds of all five muscles

studied were compared within each of the four categories by fitting separate linear mixed models with muscle (Add, RF, TA, Ham, TS) as fixed factor and subject as random factor. All post-hoc pairwise comparisons were Bonferroni corrected to adjust for multiple comparisons. Finally, we explored for a potential association between category and pathology (traumatic SCI vs. non-SCI) by conducting a χ^2 -test of independence. For this test, we considered bipolar electrode setups only, as monopolar EES was only applied in the SCI group.

To test for an association between category and electrode setup (bipolar stimulation with the cathode either rostral or caudal to the anode and with wide, intermediate, and narrow fields, or monopolar stimulation), we conducted a χ^2 -test of independence. Narrow fields were defined as bipolar stimulation with a cathode-anode separation of 4 mm or 6 mm, intermediate fields with 11 mm, 15 mm, or 18 mm, and wide fields with 24 mm, 25 mm, or 33 mm. The thresholds of RF and TS responses, respectively, were compared between bipolar wide, intermediate, and narrow fields, and monopolar stimulation using separate Kruskal-Wallis tests.

Mapping of the lumbosacral spinal cord by means of response amplitudes

We analyzed the peak-to-peak amplitudes of the EMG responses evoked by all tested electrode setups at threshold (evoking either RF or TS responses), common threshold (evoking RF and TS responses), as well as maximum stimulation. For each setup and stimulation amplitude, we obtained mean peak-to-peak amplitudes for the five muscles per leg from all available responses and normalized them to the maximum in the respective muscles obtained across all electrode setups tested in the same recording. Median normalized peak-to-peak amplitudes across subjects were calculated for the RF-bias, non-selective, and TS-bias categories for threshold, common threshold, and maximum stimulation. We excluded data sets with no RF and TS responses, a stimulation frequency > 2.5 Hz, less than four incremental stimulation amplitudes available, or the occurrence of spasms intervening with the evoked responses, reducing data sets for analysis to 394 derived from 19 subjects with traumatic SCI and six non-SCI subjects. Normalized peak-to-peak amplitudes of the five muscles at common threshold were compared per category by separate linear mixed models with muscle (Add, RF, TA, Ham, TS) as fixed factor and subject as random factor. All post-hoc pairwise comparisons were Bonferroni corrected.

Spinal cord maps of motoneuron pool activation were calculated based on RF and TS responses. Motoneuron pool activation of L2–L4 segments was derived from the product of the innervation probability of RF and the median normalized RF peak-to-peak amplitudes, that of L5–S2 segments from the product of the innervation probabilities of gastrocnemius and soleus and the median normalized TS peak-to-peak amplitudes (resulting in two separate activation maps for the TS muscles group). For the RF-bias category, we conducted separate χ^2 -tests of independence to examine potential associations between attainable EMG amplitudes of the evoked responses and pathology (traumatic SCI, N = 19; vs. non-SCI, N = 6) and severity of traumatic SCI (motor-complete SCI, AIS A and B, N = 13; vs. motor-incomplete SCI, AIS C and D, N = 6), respectively.

Intra- and postoperative comparisons

Eighty-two pairs of data sets in which the same electrode setups were tested intra- as well as postoperatively were available from 16 subjects (traumatic SCI, N = 8). We conducted a χ^2 -test of independence to test for an association between the RF- and TS-threshold based categories in prone and supine positions. RF- and TS-response thresholds, respectively, evoked in prone and supine were compared pairwise by Wilcoxon signed-rank tests.

Comparison of responses evoked by midline- and laterally placed electrodes

Data derived from subjects 2, 12, and 16 allowed to map the spinal cord by midline- as well as laterally placed electrodes. Forty-nine pairs of data sets were available with the active midline and lateral anode and cathode positions of the tested bipolar combinations at the same rostrocaudal levels. Twenty-seven of these pairs were derived with electrodes at the T12, and 22 with electrodes at the L1-vertebral level. The relationship between the RF- and TS-threshold based categories of the respective midline and lateral electrodes was evaluated descriptively.

Statistical analysis

Statistical analysis was performed using IBM SPSS Statistics 26.0 for Windows (IBM Corporation, Armonk, NY, USA). Specific tests conducted are identified in the respective paragraphs of the Results and Transparent Methods. Assumptions of normality were tested using Shapiro-Wilk tests. Descriptive statistics are reported as mean \pm SE for normally distributed data and as median and IQR for non-parametric distributions. Boxplots illustrate medians as bold horizontal lines within boxes spanning the IQR, and whiskers extending to the smallest and largest values that are not outliers (values 1.5–3 times the IQR; plotted as circles) or extreme values (values > 3 times the IQR; asterisks). Before running mixed ANOVAs, assumptions of sphericity were tested with Mauchly's tests and, if voided, Greenhouse-Geisser correction was applied. Effect sizes were reported by the partial eta-squared (η_p^2) for the ANOVAs, else by the correlation coefficient r . The strength of associations was indicated by Cramer's V . α -errors of $P < .05$ were considered significant. All post-hoc tests were Bonferroni corrected. Adjusted residuals with absolute values > 2 were considered to indicate significant deviations from independence.

Supplemental Data

The epidurally evoked responses are PRM reflexes

Figure S2A illustrates the recovery cycles of RF and TS responses to double stimuli, separately for the four amplitude categories considered. With respect to RF, the mixed ANOVA of the normalized response amplitudes demonstrated a significant interaction between amplitude category and interstimulus interval ($F(12,520) = 7.205$, $P < .001$, $\eta_p^2 = .273$). Amplitude category was a significant main effect ($F(3,520) = 18.007$, $P < .001$, $\eta_p^2 = .104$) as was the interstimulus interval ($F(4,520) = 100.752$, $P < .001$, $\eta_p^2 = .783$). Post-hoc comparisons revealed significantly stronger depression at threshold amplitude compared to the other amplitude categories as well as at the shortest interstimulus intervals

of 41 ms and 57 ms compared to the other intervals (all $P < .001$). In the case of TS, the interaction between amplitude category and interstimulus interval was also significant ($F(12,470) = 2.180$, $P = .012$, $\eta_p^2 = .092$). There was no significant main effect of amplitude category ($F(3,470) = 1.290$, $P = .277$, $\eta_p^2 = .008$) but of interstimulus interval ($F(4,470) = 127.094$, $P < .001$, $\eta_p^2 = 1.093$). Post-hoc comparisons demonstrated significant differences in-between all interstimulus intervals studied (all $P < .001$) except between the two longest intervals of 175 ms and 445 ms.

We investigated whether the reduced depression of RF responses with stimulation amplitudes above threshold would be related to the elicitation of a direct M wave-like response component, which would not show post-stimulation depression. Were that the case, concomitant electrical stimulation of anterior root-motor axons would reduce the response latency by a minimum of 1.5 ms compared with threshold responses (Dimitrijevic et al., 1983; Halter et al., 1983). The onset latencies of the unconditioned first RF responses of the pairs evoked with an interstimulus interval of 41 ms (Figure S2B) showed no differences between the four amplitude categories (Kruskal-Wallis test, $\chi^2(3) = .691$, $P = .875$, $r = .108$). Median values (IQR) were 10.0 ms (9.5–10.5), 10.0 ms (9.0–10.5), 10.5 ms (9.5–11.0), and 10.5 ms (10.0–10.5). The reduced depression in RF with stimulation above threshold may be related to the reflex-size dependence of post-stimulation depression (Kagamiyara et al., 1998). The interpretation that anterior roots were not electrically stimulated can be generalized to all studied muscles, because the RF and TS responses tested all roots from L2–S2.

Laterally located electrodes can lead to a dissociation between segmental cathode sites and activated spinal cord segments

Figure S3A shows exemplary results of RF- and TS-PRM reflexes evoked with midline- and laterally placed cathodes at the upper third of the T12 and at the middle third of the L1-vertebral body level, respectively. Sketches of the active cathode-anode combinations with respect to the spinal cord and root anatomy illustrate our hypothesis that lateral stimulation over the terminal spinal cord may lead to stimulation of posterior roots of passage, and hence to a dissociation between the segmental stimulation site and the activated spinal cord segments. Lateral cathodes previously demonstrated to recruit ipsilateral S1/S2 roots at threshold (Wagner et al., 2018) were likely located at the level of the respective spinal cord segments, i.e., more rostrally than in the example given here. The relationship between the RF- and TS-threshold based categories associated with midline- and laterally located electrode locations of the available data sets are displayed in Figure S3B and specified in Table S9.

Supplemental References

- Berry, J.L., Moran, J.M., Berg, W.S., and Steffee, A.D. (1987). A Morphometric Study of Human Lumbar and Selected Thoracic Vertebrae. *Spine (Phila. Pa. 1976)*. 12, 362–367.
- Bing, R. (1948). *Kompendium der topischen Gehirn- und Rückenmarksdiagnostik*, 14th ed (Benno Schwabe & Co. Verlag).
- Busscher, I., Ploegmakers, J.J.W., Verkerke, G.J., and Veldhuizen, A.G. (2010). Comparative anatomical dimensions of the complete human and porcine spine. *Eur. Spine J.* 19, 1104–1114.
- Capogrosso, M., Wenger, N., Raspopovic, S., Musienko, P., Beauparlant, J., Bassi Luciani, L., Courtine, G., and Micera, S. (2013). A computational model for epidural electrical stimulation of spinal sensorimotor circuits. *J. Neurosci. Off. J. Soc. Neurosci.* 33, 19326–19340.
- Cotterill, P.C., Kostuik, J.P., D'Angelo, G., Fernie, G.R., and Maki, B.E. (1986). An anatomical comparison of the human and bovine thoracolumbar spine. *J. Orthop. Res.* 4, 298–303.
- Cunningham, D. (1991). *Cunningham's textbook of anatomy*, 12th ed (Oxford University Press).
- d'Avella, D., and Mingrino, S. (1979). Microsurgical anatomy of lumbosacral spinal roots. *J. Neurosurg.* 51, 819–823.
- DeJong, R. (1979). *The neurologic examination: incorporating the fundamentals of neuroanatomy and neurophysiology*, 4th ed (Haper & Row).
- Demir, M., Atay, E., Seringeç, N., Yoldaş, A., Çiçek, M., Ertoğrul, R., and Güneri, B. (2018). Intervertebral disc heights and concavity index of the lumbar spine in young healthy adults. *Anatomy* 12, 34–37.
- Demiryürek, D., Aydingöz, Ü., Akşit, M.D., Yener, and N., Geyik, P.Ö. (2002). MR imaging determination of the normal level of conus medullaris. *Clin. Imaging* 26, 375–377.
- Dimitrijevic, M.R., Faganel, J., and Sherwood, A.M. (1983). Spinal cord stimulation as a tool for physiological research. *Appl. Neurophysiol.* 46, 245–253.
- Donaldson, H.H., and Davis, D.J. (1903). A description of charts showing the areas of the cross sections of the human spinal cord at the level of each spinal nerve. *J. Comp. Neurol.* 13, 19–40.
- Ellis, H., Logan, B., and Dixon, A. (1999). *Human sectional anatomy*, 2nd ed (Butterworth-Heinemann).
- Fang, D., Cheung, K.M.C., Ruan, D., Chan, F.L. (1994). Computed Tomographic Osteometry of the Asian Lumbar Spine. *J. Spinal Disord.* 7, 307–316.
- Fletcher, J.G.R., Stringer, M.D., Briggs, C.A., Davies, T.M., and Woodley, S.J. (2015). CT morphometry of adult thoracic intervertebral discs. *Eur. Spine J.* 24, 2321–2329.
- Foerster, O., and Bumke, O. (1936). *Handbuch der Neurologie* (Springer).
- Forseen, S., and Borden, N. (2015). *Imaging Anatomy of the Human Spine* (Springer Publishing Company).
- Frost, B., Camarero-Espinosa, S., and Foster, E. (2019). Materials for the Spine: Anatomy, Problems, and Solutions. *Materials (Basel)*. 12, 253.
- Gray, H. (1989). *Gray's anatomy*, 37th ed. (Churchill Livingstone).
- Gybels, J., and Van Roost, D. (1985). Spinal cord stimulation for the modification of dystonic and hyperkinetic conditions: A critical Review. In *Upper Motor Neuron Functions and Dysfunctions. Recent Achievements in Restorative Neurology*, J. Eccles, M.R. Dimitrijevic, eds. (S Karger AG), pp. 58–70.
- Halter, J., Dolenc, V., Dimitrijevic, M.R., and Sharkey, P.C. (1983). Neurophysiological assessment of electrode placement in the spinal cord. *Appl. Neurophysiol.* 46, 124–128.
- Hauck, E.F., Wittkowski, W., and Bothe, H.W. (2008). Intradural microanatomy of the nerve roots S1–S5 at their origin from the conus medullaris. *J. Neurosurg. Spine* 9, 207–212.
- Haymaker, W., and Woodhall, B. (1953). *Peripheral Nerve Injuries*, 2nd ed. (W. B. Saunders Company).
- Hofstoetter, U.S., Freundl, B., Binder, H., and Minassian, K. (2018). Common neural structures activated by epidural and transcutaneous lumbar spinal cord stimulation: Elicitation of posterior root-muscle reflexes. *PLoS One* 13, e0192013.
- Hofstoetter, U.S., Freundl, B., Binder, H., and Minassian, K. (2019). Recovery cycles of posterior root-muscle reflexes evoked by transcutaneous spinal cord stimulation and of the H reflex in individuals with intact and injured spinal cord. *PLoS One* 14, e0227057.
- Holsheimer, J., den Boer, J.A., Struijk, J.J., and Rozeboom, A.R. (1994). MR assessment of the normal position of the spinal cord in the spinal canal. *AJNR. Am. J. Neuroradiol.* 15, 951–959.
- Huk, W., Gademann, G., and Friedmann, G. (1990). *Magnetic resonance imaging of central nervous system diseases: functional anatomy - imaging, neurological symptoms - pathology* (Springer).

- Kagamihara, Y., Hayashi, A., Okuma, Y., Nagaoka, M., Nakajima, Y., and Tanaka, R. (1998). Reassessment of H-reflex recovery curve using the double stimulation procedure. *Muscle Nerve* 21, 352–360.
- Karabulut, O., Akay, H., Karabulut, Z., Özevren, H., Saka, G., Hatipoglu, S., and Devenci, E. (2016). Conus Medullaris Position in an Adult Population: Analysis of Magnetic Resonance Imaging. *Int. J. Morphol.* 34, 1352–1356.
- Kim, J.T., Bahk, J.H., and Sung, J. (2003). Influence of Age and Sex on the Position of the Conus Medullaris and Tuffier's Line in Adults. *Anesthesiology* 99, 1359–1363.
- Ko, H.-Y., Park, J.H., Shin, Y.B., and Baek, S.Y. (2004). Gross quantitative measurements of spinal cord segments in human. *Spinal Cord* 42, 35–40.
- Koeller, W., Meier, W., and Hartmann, F. (1984). Biomechanical Properties of Human Intervertebral Discs Subjected to Axial Dynamic Compression. *Spine (Phila. Pa. 1976)*. 9, 725–733.
- Krag, M., Weaver, D., Beynon, B., and Haugh, L. (1988). Morphometry of the Thoracic and Lumbar Spine Related to Transpedicular Screw Placement for Surgical Spinal Fixation. *Spine (Phila. Pa. 1976)*. 13, 27–32.
- Kunkel, M.E., Herkommer, A., Reinehr, M., Böckers, T.M., and Wilke, H.-J. (2011). Morphometric analysis of the relationships between intervertebral disc and vertebral body heights: an anatomical and radiographic study of the human thoracic spine. *J. Anat.* 219, 375–387.
- Küper, K. (2001). *MR/ CT-Atlas der Anatomie*. Georg Thieme Verlag.
- Kwon, S., Kim, T.S., Kim, H.S., and Rhyu, I.J. (2016). The Tip Level of the Conus Medullaris by Magnetic Resonance Imaging and Cadaver Studies in Korean Adults. *Korean J. Phys. Anthropol.* 29, 47.
- Lang, J. (1984). Morphologie und funktionelle Anatomie der Lendenwirbelsäule und des benachbarten Nervensystems - 1. Rückenmark. In *Neuroorthopädie 2 – Lendenwirbelsäulenerkrankungen mit Beteiligung des Nervensystems*, D. Hohmann, B. Kügelgen, K. Liebig, M. Schirmer, eds. (Springer), pp. 3–9.
- Laporte, S., Mitton, D., Ismael, B., de Fouchecour, M., Lasseau, J.P., Lavaste, F., and Skalli, W. (2000). Quantitative morphometric study of thoracic spine A preliminary parameters statistical analysis. *Eur. J. Orthop. Surg. Traumatol.* 10, 85–91.
- Liguori, R., Krarup, C., and Trojaborg, W. (1992). Determination of the segmental sensory and motor innervation of the lumbosacral spinal nerves: An electrophysiological study. *Brain* 115, 915–934.
- Liu, A., Yang, K., Wang, D., Li, C., Ren, Z., Yan, S., Buser, Z., and Wang, J.C. (2017). Level of conus medullaris termination in adult population analyzed by kinetic magnetic resonance imaging. *Surg. Radiol. Anat.* 39, 759–765.
- Magladery, J., Teasdall, R., Park, A., and Porter, W. (1951). Electrophysiological studies of nerve and reflex activity in normal man. V. Excitation and inhibition of two-neurone reflexes by afferent impulses in the same trunk. *Bull. Johns Hopkins Hosp.* 88, 520–537.
- Mersdorf, A., Schmidt, R.A., and Tanagho, E.A. (1993). Topographic-Anatomical Basis of Sacral Neurostimulation: Neuroanatomical Variations. *J. Urol.* 149, 345–349.
- Minassian, K., Jilge, B., Rattay, F., Pinter, M.M., Binder, H., Gerstenbrand, F., and Dimitrijevic, M.R. (2004). Stepping-like movements in humans with complete spinal cord injury induced by epidural stimulation of the lumbar cord: electromyographic study of compound muscle action potentials. *Spinal Cord* 42, 401–416.
- Minassian, K., McKay, W.B., Binder, H., and Hofstoetter, U.S. (2016). Targeting Lumbar Spinal Neural Circuitry by Epidural Stimulation to Restore Motor Function After Spinal Cord Injury. *Neurotherapeutics* 13, 284–294.
- Moon, M.S., Jeong, J.H., Kim, S.J., Kim, M.S., and Choi, W.R. (2019). Magnetic resonance imaging observations of the conus medullaris in a Korean population. *Asian Spine J.* 13, 313–317.
- Moussallem, C.D., El Masri, H., El-Yahouchi, C., Abou Fakher, F., and Ibrahim, A. (2014). Relationship of the Lumbar Lordosis Angle to the Level of Termination of the Conus Medullaris and Thecal Sac. *Anat. Res. Int.* 2014, 1–4.
- Nasr, A.Y. (2016). Vertebral level and measurements of conus medullaris and dural sac termination with special reference to the apex of the sacral hiatus: Anatomical and magnetic resonance imaging radiologic study. *Folia Morphol.* 75, 287–299.
- Nissan, M., and Gilad, I. (1984). The Cervical and Lumbar Vertebrae — An Anthropometric Model. *Eng. Med.* 13, 111–114.

- Panjabi, M.M., Goel, V., Oxland, T., Takata, K., Duranceau, J., Krag, M., and Price, M. (1992). Human lumbar vertebrae. Quantitative three-dimensional anatomy. *Spine (Phila. Pa. 1976)*. 17, 299–306.
- Panjabi, M.M., Takata, K., Goel, V., Federico, D., Oxland, T., Duranceau, J., and Krag, M. (1991). Thoracic human vertebrae. Quantitative three-dimensional anatomy. *Spine (Phila. Pa. 1976)*. 16, 888–901.
- Phillips, L.H., and Park, T.S. (1991). Electrophysiologic mapping of the segmental anatomy of the muscles of the lower extremity. *Muscle Nerve* 14, 1213–1218.
- Pierrot-Deseilligny, E., and Burke, D. (2012). *The Circuitry of the Human Spinal Cord* (Cambridge University Press).
- Pinter, M.M., Gerstenbrand, F., and Dimitrijevic, M.R. (2000). Epidural electrical stimulation of posterior structures of the human lumbosacral cord: 3. Control Of spasticity. *Spinal Cord* 38, 524–531.
- Pomeranz, S.J. (1992). *MRI total body atlas, volume 1* (MRI Education Foundation)
- Preeti, and Chaturvedi, M. (2016). MRI Study of Level of Termination of Spinal Cord (Conus Medullaris). *Int. J. Sci. Res.* 5, 122–124.
- Rostamzadeh, A., Amiri, M., Joghataei, M.T., and Fatehi, D. (2015). Prevention of diagnostic errors in position of conus medullaris in adult patients. *Int. J. Epidemiol. Res.* 2, 118–125.
- Saifuddin, A., Burnett, S.J.D., and White, J. (1998). The variation of position of the conus medullaris in an adult population. A magnetic resonance imaging study. *Spine (Phila. Pa. 1976)* 23, 1452–1456.
- Schirmer, C.M., Shils, J.L., Arle, J.E., Cosgrove, G.R., Dempsey, P.K., Tarlov, E., Kim, S., Martin, C.J., Feltz, C., Moul, M., et al. (2011). Heuristic map of myotomal innervation in humans using direct intraoperative nerve root stimulation. *J. Neurosurg. Spine* 15, 64–70.
- Schnitzlein, H.N., and Murtagh, F.R. (1990). *Imaging anatomy of the head and spine: A photographic color atlas of MRI, CT, gross, and microscopic anatomy axial, coronal, and sagittal planes*, 2nd ed. (Urban & Schwarzenberg).
- Scoles, P. V., Linton, A.E., Latimer, B., Levy, M.E., and Digiovanni, B.F. (1988). Vertebral Body and Posterior Element Morphology. *Spine (Phila. Pa. 1976)*. 13, 1082–1086.
- Sevinc, O., Is, M., Barut, C., Eryoruk, N., Kiran, S., and Arifoglu, Y. (2006). MRI determination of conus medullaris level in an adult population in Turkey. *Neuroradiol. J.* 19, 375–378.
- Sharrard, W.J. (1964). The Segmental Innervation of the Lower Limb Muscles in Man. *Ann. R. Coll. Surg. Engl.* 35, 106–122.
- Singh, R., Srivastva, S.K., Prasath, C.S.V., Rohilla, R.K., Siwach, R., and Magu, N.K. (2011). Morphometric Measurements of Cadaveric Thoracic Spine in Indian Population and Its Clinical Applications. *Asian Spine J.* 5, 20–34.
- Spalteholz, W. (1923). *Hand-Atlas of Human Anatomy*, 4th ed. (Lippincott Company).
- Tan, S.H., Teo, E.C., and Chua, H.C. (2004). Quantitative three-dimensional anatomy of cervical, thoracic and lumbar vertebrae of Chinese Singaporeans. *Eur. Spine J.* 13, 137–146.
- Thage, O. (2009). The myotomes L2-S2 in man. *Acta Neurol. Scand.* 41, 241–244.
- Uhlenbrock, D. (2001). *MRT der Wirbelsäule und des Spinalkanals*. (Thieme).
- Wagner, F.B., Mignardot, J.-B., Le Goff-Mignardot, C.G., Demesmaeker, R., Komi, S., Capogrosso, M., Rowald, A., Seáñez, I., Caban, M., Pirondini, E., et al. (2018). Targeted neurotechnology restores walking in humans with spinal cord injury. *Nature* 563, 65–71.
- Weyreuther, M., Heyde, C.E., Westphal, M., Zierski, J., and Weber, U. (2007). *MRI Atlas: Orthopedics and Neurosurgery: The Spine*. (Springer).
- Yamada, S., Perot, P.L., Ducker, T.B., and Lockard, I. (1976). Myelotomy for control of mass spasms in paraplegia. *J. Neurosurg.* 45, 683–691.